

### Public Domain Mark 1.0 Universal

This work was written as part of one of the author's official duties as an Employee of the United States Government and is therefore a work of the United States Government. In accordance with 17 U.S.C. 105, no copyright protection is available for such works under U.S. Law.

Access to this work was provided by the University of Maryland, Baltimore County (UMBC) ScholarWorks@UMBC digital repository on the Maryland Shared Open Access (MD-SOAR) platform.

### **Please provide feedback**

Please support the ScholarWorks@UMBC repository by emailing [scholarworks-group@umbc.edu](mailto:scholarworks-group@umbc.edu) and telling us what having access to this work means to you and why it's important to you. Thank you.

# Earth and Space Science



## RESEARCH ARTICLE

10.1029/2022EA002473

### Key Points:

- Shipboard Pandora NO<sub>2</sub> columns and surface O<sub>3</sub>, NO<sub>2</sub>, CO, and volatile organic compounds (VOCs) over the Gulf of Mexico (GOM), May 2019, displayed two air quality (AQ) regimes
- GOM AQ was dominated by continental NO<sub>2</sub> sources and near-shore VOC; deepwater oil platforms were in a clean marine regime
- Pandora and satellite total column NO<sub>2</sub> over GOM agreed overall within 5% in clean, clear-sky conditions along the coast and 13% over water

### Supporting Information:

Supporting Information may be found in the online version of this article.

### Correspondence to:

A. M. Thompson,  
[anne.m.thompson@nasa.gov](mailto:anne.m.thompson@nasa.gov)

### Citation:

Thompson, A. M., Kollonige, D. E., Stauffer, R. M., Kotsakis, A. E., Abuhassan, N., Lamsal, L. N., et al. (2023). Two air quality regimes in total column NO<sub>2</sub> over the Gulf of Mexico in May 2019: Shipboard and satellite views. *Earth and Space Science*, 10, e2022EA002473. <https://doi.org/10.1029/2022EA002473>








Received 18 JUN 2022

Accepted 6 FEB 2023

### Author Contributions:

**Conceptualization:** Anne M. Thompson  
**Data curation:** Debra E. Kollonige, Lok N. Lamsal, Donald R. Blake, Amy Townsend-Small

## Two Air Quality Regimes in Total Column NO<sub>2</sub> Over the Gulf of Mexico in May 2019: Shipboard and Satellite Views

Anne M. Thompson<sup>1,2</sup> , Debra E. Kollonige<sup>1,3</sup> , Ryan M. Stauffer<sup>1</sup> , Alexander E. Kotsakis<sup>1,4</sup> , Nader Abuhassan<sup>1,2</sup>, Lok N. Lamsal<sup>1,2</sup> , Robert J. Swap<sup>1</sup>, Donald R. Blake<sup>5</sup> , Amy Townsend-Small<sup>6</sup> , and Holli D. Wecht<sup>7</sup>

<sup>1</sup>Earth Sciences Division, NASA/Goddard Space Flight Center, Greenbelt, MD, USA, <sup>2</sup>GESTAR and Joint Center for Earth Systems Technology, University of Maryland, Baltimore County, Baltimore, MD, USA, <sup>3</sup>SSAI, Lanham, MD, USA, <sup>4</sup>ERT, Inc., Laurel, MD, USA, <sup>5</sup>Department of Chemistry, University of California Irvine, Irvine, CA, USA, <sup>6</sup>Department of Geology and Geography, University of Cincinnati, Cincinnati, OH, USA, <sup>7</sup>Bureau of Ocean Energy Management, Office of Environmental Programs, Sterling, VA, USA

**Abstract** The Satellite Coastal and Oceanic Atmospheric Pollution Experiment (SCOAPE) cruise in the Gulf of Mexico was conducted in May 2019 by NASA and the Bureau of Ocean Energy Management to determine the feasibility of using satellite data to measure air quality in a region of concentrated oil and natural gas (ONG) operations. SCOAPE addressed both technological and scientific issues related to measuring NO<sub>2</sub> columns over the outer continental shelf. Featured were nitrogen dioxide (NO<sub>2</sub>) instruments (Pandora, Teledyne API analyzer) at Cocodrie, LA (29.26°, −90.66°), and on the *Research Vessel Point Sur* operating off the Louisiana coast with measurements of ozone, carbon monoxide, and volatile organic compounds (VOCs). The findings: (a) all NO<sub>2</sub> observations revealed two atmospheric regimes over the Gulf, the first influenced by tropical air in 10–14 May, the second influenced by flow from urban areas on 15–17 May; (b) comparisons of OMI v4 and TROPOMI v1.3 TC (total column) NO<sub>2</sub> data with shipboard Pandora NO<sub>2</sub> column observations averaged 13% agreement with the largest difference during 15–17 May (~20%). At Cocodrie, the satellite–Pandora agreement was ~5%. (c) Three new-model Pandora instruments displayed a TC NO<sub>2</sub> precision of 0.01 Dobson Units (~5%); (d) regions of smaller, older natural gas operations showed high methane readings from leakage; elevated VOCs were also detected. Neither satellite nor spectrometer captured the magnitude of ambient NO<sub>2</sub> variability near ONG platforms. Given an absence of regular air quality monitoring over the Gulf of Mexico, SCOAPE data constitute a baseline against which future observations can be compared.

**Plain Language Summary** The Satellite Coastal and Oceanic Atmospheric Pollution Experiment (SCOAPE) cruise in the Gulf of Mexico (GOM) conducted on the *Research Vessel Point Sur* in May 2019 investigated the feasibility of using satellite data to measure air quality in a region of concentrated oil and natural gas (ONG) operations. SCOAPE addressed both technological and scientific issues related to measuring NO<sub>2</sub> columns in a prototypical coastal environment. The results are as follows. First, measurements from SCOAPE demonstrated that satellite NO<sub>2</sub> data can be used to monitor ONG activity over the GOM. Second, during SCOAPE both OMI and TROPOMI TC (total column) NO<sub>2</sub> amounts were higher over land and sometimes the near-shore ONG-rich Gulf, than over deepwater regions farther offshore. This was confirmed by Pandora spectrometer “ground truth” TC NO<sub>2</sub> data measured throughout SCOAPE on shore and on ship. Third, SCOAPE established the reliability and precision of a new generation of Pandora spectrometers. Fourth, comparisons of satellite and Pandora TC NO<sub>2</sub> data in SCOAPE confirm previous land–water interface studies that point to limitations in satellite NO<sub>2</sub> in coastal regions. Finally, neither satellite nor spectrometer captures the magnitude of ambient (“nose-level”) NO<sub>2</sub> variability in a region dotted with hundreds of ONG platforms.

## 1. Introduction

### 1.1. Background

Within the past decade, there have been several focused studies of air quality (AQ) along North American coastlines where pollutants display distinct air–water gradients due to interactions of complex marine meteorology with rapidly reacting chemical constituents. Because satellite data are viewed as fundamental to large-regional AQ observations, the sampling strategies of these campaigns include space-borne sensors that may be tested to the limit in terms of detection thresholds, accuracy, and precision. Experimental designs complement the

© 2023 The Authors. Earth and Space Science published by Wiley Periodicals LLC on behalf of American Geophysical Union.

This is an open access article under the terms of the [Creative Commons Attribution License](https://creativecommons.org/licenses/by/4.0/), which permits use, distribution and reproduction in any medium, provided the original work is properly cited.

**Formal analysis:** Anne M. Thompson, Debra E. Kollonige, Ryan M. Stauffer, Alexander E. Kotsakis, Nader Abuhassan, Lok N. Lamsal, Donald R. Blake, Amy Townsend-Small

**Funding acquisition:** Anne M. Thompson, Ryan M. Stauffer, Robert J. Swap, Holli D. Wecht

**Investigation:** Debra E. Kollonige, Ryan M. Stauffer, Alexander E. Kotsakis, Nader Abuhassan, Donald R. Blake

**Methodology:** Anne M. Thompson, Debra E. Kollonige, Alexander E. Kotsakis, Lok N. Lamsal, Robert J. Swap

**Resources:** Anne M. Thompson, Robert J. Swap, Donald R. Blake, Holli D. Wecht

**Software:** Debra E. Kollonige, Ryan M. Stauffer, Alexander E. Kotsakis, Nader Abuhassan, Lok N. Lamsal

**Validation:** Anne M. Thompson, Debra E. Kollonige, Alexander E. Kotsakis, Nader Abuhassan, Lok N. Lamsal, Robert J. Swap, Donald R. Blake, Amy Townsend-Small

**Visualization:** Debra E. Kollonige, Ryan M. Stauffer

**Writing – original draft:** Anne M. Thompson

**Writing – review & editing:** Anne M. Thompson, Debra E. Kollonige, Ryan M. Stauffer, Alexander E. Kotsakis, Nader Abuhassan, Lok N. Lamsal, Robert J. Swap, Donald R. Blake, Amy Townsend-Small, Holli D. Wecht

satellite observations with airborne, ship, and ground-based instruments that may themselves be using technology in development. Measurements from these experiments are typically used in comparisons with satellite column amounts and, in some cases, can be used to improve the satellite retrievals. Nitrogen dioxide ( $\text{NO}_2$ ) is an important constituent for remote sensing measurements because  $\text{NO}_2$  can be used as a proxy for nitrogen oxides ( $\text{NO}_x = \text{nitric oxide [NO]} + \text{NO}_2$ ), a product of combustion and a major precursor for the formation of ozone.

Satellite, airborne, and ground-based instruments for the remote sensing of  $\text{NO}_2$  have been employed for decades. For example, satellites have been measuring  $\text{NO}_2$  since the mid-1990s, starting with the GOME series (Burrows et al., 1999). These and other long-term records, for example, from Aura's OMI (Ozone Measuring Instrument), are well known for characterizing global, regional, and temporal variability (Duncan, 2020; Duncan et al., 2013, 2016; Levelt et al., 2018). Seasonal patterns and trends in  $\text{NO}_2$  as well as signatures of extreme events, for example, the 2008–2010 recession and the 2020 COVID-19 pandemic, are well documented (Goldberg et al., 2020; Russell et al., 2012; Tong et al., 2015). Airborne instrumentation used to measure column amounts and profiles of  $\text{NO}_2$  includes differential optical absorption spectroscopy (DOAS; Heue et al., 2008; Tack et al., 2019) and NASA's GEO-TASO (Nowlan et al., 2016) and GCAS (Judd et al., 2020).

## 1.2. Remote Sensing Studies of Coastal Air Quality/Overview of Recent Results

A host of ground-based UltraViolet (UV)/Visible  $\text{NO}_2$  instruments were intercompared in the Cabauw Intercomparison campaign for Nitrogen Dioxide measuring Instruments (CINDI) campaigns (Peters et al., 2012; Tzirpitz et al., 2021) and the 2019 TROPomi Validation eXperiment (TROLIX; Kreher et al., 2020). The Pandora spectrometer is a relatively new ground-based spectrometer (Herman et al., 2009, 2018) that has been used to measure column  $\text{NO}_2$  in several coastal experiments: CAPABLE (Knepp et al., 2015) in 2010–2011, DISCOVER-AQ in Maryland in July 2011 (Reed et al., 2015; Tzortziou, Herman, et al., 2015), DISCOVER-AQ in Houston in 2013 (Judd et al., 2019), DANCE in 2014 off the Virginia and North Carolina coast (Kollonige et al., 2018; Martins et al., 2016), KORUS-OC in 2016 around the Korean peninsula (Thompson, Stauffer, et al., 2019; Tzortziou, Thompson, et al., 2015; Tzortziou et al., 2018), OWLETS-1 in 2017 in the lower Chesapeake Bay (Gronoff et al., 2019; Sullivan et al., 2018), OWLETS-2 in 2018 in the upper Chesapeake Bay (Kotsakis et al., 2022; Sullivan et al., 2020), LMOS in 2017 (Stanier et al., 2021), and LISTOS (Long Island Sound) in 2018 (Judd et al., 2020; Karambelas, 2020). Table 1 gives a list of campaigns and experiments that preceded Satellite Coastal and Oceanic Atmospheric Pollution Experiment (SCOAPE). A summary of findings from these studies is as follows:

- Agreement between the sun-tracking Pandora and satellite TC  $\text{NO}_2$  with satellite varies depending on viewing geometry (Verhoelst et al., 2021). The satellite footprint size at nadir is  $\sim 13 \times 24$  km for OMI and  $3.5 \times 7.2$  km for TROPOMI during field campaigns in 2018 through July 2019. In general, agreement of Pandora TC  $\text{NO}_2$  is closer to TROPOMI than for OMI, especially if the larger satellite pixel includes considerable spatial heterogeneity (Thompson, 2020; Thompson et al., 2020).
- At very polluted locations, as TC  $\text{NO}_2$  measured from the surface increases, there tends to be greater disagreement with the corresponding satellite TC  $\text{NO}_2$  (Herman et al., 2019). This can be due to the heterogeneity of a region Pandora senses as polluted.
- Besides comparing  $\text{NO}_2$  column amounts from satellite or another instrument to the Pandora, the relationship between continuous surface  $\text{NO}_2$  and Pandora TC  $\text{NO}_2$  in coastal environments has been investigated (Knepp et al., 2015; Kollonige et al., 2018; Martins et al., 2016; Thompson, Stauffer, et al., 2019). Correlations between time-coincident surface  $\text{NO}_2$  and Pandora TC  $\text{NO}_2$  vary considerably. Causes of the divergence may be meteorological, for example, when the Pandora senses an  $\text{NO}_2$ -rich residual layer located above a relatively unpolluted boundary layer (Kotsakis et al., 2022). Cloud interferences in remotely sensed columns tend to be important along coastlines. In shipboard experiments, the in situ instrument may be detecting plumes that are not in the field of view (FOV) of the Pandora (Thompson, Stauffer, et al., 2019).

## 1.3. SCOAPE Background and Scientific Issues

None of the experiments described in Table 1 were based on comprehensive AQ measurements over a major body of water. The SCOAPE cruise, designed by NASA's Goddard Space Flight Center (GSFC) and the Department of the Interior's Bureau of Ocean Energy Management (BOEM), offered an opportunity to study  $\text{NO}_2$  pollution over

**Table 1**  
*List of Relevant Campaigns and Experiments That Preceded SCOAPE*

Campaign (year(s))	Geographic location	Reference
CAPABLE (2009, 2010, 2011)	Hampton, VA	Martins et al. (2012) Knepp et al. (2015)
DISCOVER-AQ MD (2011)	Baltimore, MD; Washington, DC	Reed et al. (2015) Tzortziou, Herman, et al. (2015)
DISCOVER-AQ TX (2013)	Houston, TX	Flynn et al. (2014) Nowlan et al. (2016) Judd et al. (2019)
DANCE (2014)	Atlantic Coast (DE-NC)	Martins et al. (2016) Kollonige et al. (2018)
KORUS-OC (2016)	Southern Korean peninsula	Tzortziou et al. (2018) Tzortziou, Thompson, et al. (2015); Thompson, Stauffer, et al. (2019)
LMOS (2017)	Lake Michigan	Adelman et al. (2020) Stanier et al. (2021)
OWLETS (2017)	Hampton, VA; Lower Chesapeake Bay	Sullivan et al. (2018) Gronoff et al. (2019) Dacic et al. (2020)
OWLETS-2 (2018)	Baltimore, MD; Upper Chesapeake Bay	Sullivan et al. (2020) Kotsakis et al. (2022)
LISTOS (2018)	Long Island Sound, NY	Judd et al. (2020) Karambelas (2020)

the Gulf of Mexico (GOM). BOEM issues leases for oil and natural gas (ONG) exploration in the outer continental shelf (OCS; 3–200 nm [5.4–370 km] off Louisiana and Alabama) of the GOM and has jurisdiction over AQ west of 87.5°W. Based on fuel usage reported by energy, shipping, and other industries over the central and western GOM, BOEM compiles estimates for NO<sub>2</sub>, SO<sub>2</sub>, and volatile organic compound (VOC) emissions in the region (Wilson et al., 2017, 2019). However, there are no AQ monitors over the GOM. In the past decade, NASA has refined OMI and other satellite products aimed at regional AQ (e.g., Boersma et al., 2018; Lamsal et al., 2014, 2017, 2021). TROPOMI NO<sub>2</sub> products have been reported by Goldberg et al. (2021). At the same time, since 2018 upgraded models of the Pandora instrument (Kotsakis et al., 2022; Robinson et al., 2020; Spinei et al., 2021) have been deployed to evaluate OMI and TROPOMI satellite products.

The SCOAPE campaign collected GOM pollution data for the first time while advancing both satellite and Pandora capabilities. A ship cruise was designed for assessing satellite capability for the measurement of trace species required to characterize GOM AQ off the eastern Louisiana coast where ONG exploration, extraction, and production activities are heavily concentrated. In addition to BOEM's emissions database, meteorological and logistical considerations (avoiding winter storms, late summer hurricanes) determined the sampling strategy. Onshore flow was desired to be able to detect air masses arriving from the Gulf. Because both satellite and the Pandora spectrometer operate in the near UV–Visible region, minimizing cloud cover was a criterion for logistics. May 2019 was selected; climatology shows less cloudiness and more onshore flow in May than in June or July.

The SCOAPE cruise was planned to address the following questions:

1. What do pollutant levels measured by satellite over the GOM look like, and how do deepwater regions compare to coastal Louisiana? What role does meteorology play in any observed differences? *Both satellite and shipboard measurements of total column (TC) NO<sub>2</sub> are used to address this question.*
2. Can satellite observations detect emissions from ONG operations over the GOM and are the measurements accurate? *This is addressed by comparing TC NO<sub>2</sub> from satellite overpasses over the GOM with TC NO<sub>2</sub> from Pandora over both land and ocean.*



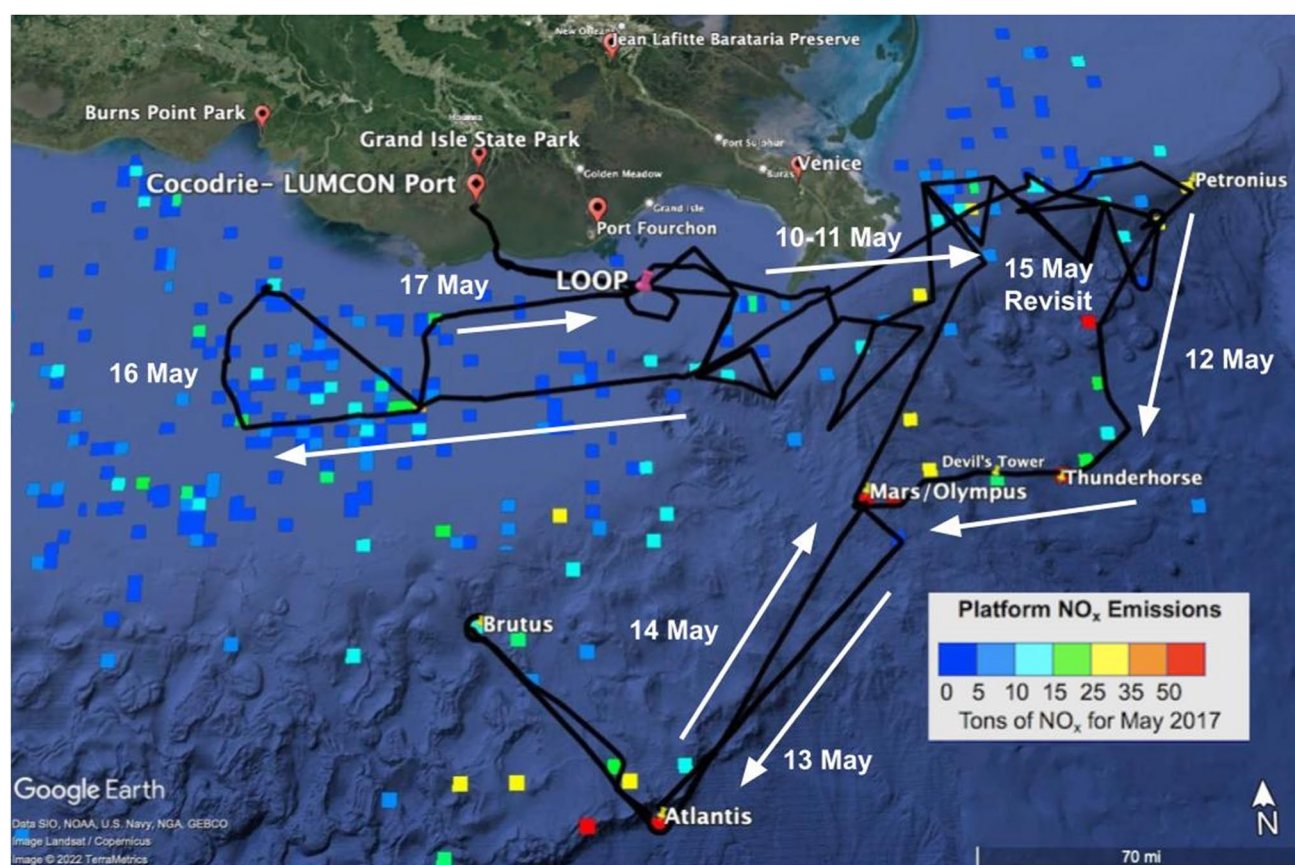


**Figure 1.** SCOAPE cruise track (black), with arrows indicating movements of *R/V Point Sur* in May 2019. Pandora calibrations were conducted at Cocodrie. Canister samples were coordinated with ship canister filling from locations in Louisiana depicted as red pins. Emissions shown for  $\text{NO}_x$  by Wilson et al. (2017, 2019) are BOEM's publicly available estimates based on monthly reports of fuel usage by operators using the Gulfwide Offshore Activities Data System (GOADS). EPA emission factors for methane, volatile organic compounds (VOCs),  $\text{SO}_2$ , CO,  $\text{CO}_2$ ,  $\text{NO}_x$ , and particulate matter are used to convert the GOADS data into the values shown here. Sources of platform  $\text{NO}_x$  emissions include diesel engines and combustion flares. Figures 4, 9, and 10 illustrate trace gases from encounters with some of the named platforms here.

3. How accurately do Pandora  $\text{NO}_2$  measurements track day-to-day variations in emissions? How precise are Pandora TC  $\text{NO}_2$  observations? *Pandora data are compared to shipboard  $\text{NO}_2$  concentrations in the vicinity of ONG operations. Precision is addressed by deploying three Pandoras together 4 weeks in advance of the cruise.*
4. Is there a difference in pollutant emissions between large, deepwater ONG platforms and the hundreds of small near-shore operations? *Whole-air samples collected near platforms are analyzed for VOC and other chemical tracers.*

Section 2 describes the design of the SCOAPE cruise, instrumentation, and ancillary data used for analysis. Section 3 presents results with interpretation and discussion. It turns out that the cruise period was characterized by two distinct meteorological regimes (Section 3.1) that were reflected in contrasting chemical composition over the GOM. Details of these regimes in terms of satellite and shipboard  $\text{NO}_2$  measurements, as well as data from other pollution tracers, appear in Sections 3.2 and 3.3. Section 4 is a summary.

## 2. Experimental: Cruise Design, Operations, Instrumentation, Ancillary Data, and Analysis

The cruise track for the *Research Vessel [R/V] Point Sur* is superimposed on the Google Earth Map (Figure 1) with land and major platform locations and color-coded  $\text{NO}_x$  emissions (Wilson et al., 2019). In addition to the LOOP (Louisiana Offshore Oil Port, an exclusion zone for research operations) and heavy commercial ship traffic—fishing, energy- and nonenergy-related—there are two basic types of ONG operations in the GOM.

Deepwater platforms, typically the largest and located farther from shore, are the most polluting individual operations, corresponding to locations color-coded yellow–orange–red in Figure 1; they primarily produce oil with accompanying natural gas flared off. Closer to shore are hundreds of older, small operations in higher density but with less  $\text{NO}_x$  emitted per platform. Most of those emitters are in blue and light blue in Figure 1.

The *R/V Point Sur* departed LUMCON (Louisiana Universities Marine Consortium; <https://lumcon.edu>) Cocodrie, LA, facility ( $29.26^\circ$ ,  $-90.66^\circ$ ) at midnight starting 10 May 2019. The ship headed east on entering the GOM, sampling in the eastern region of high-density operations (10–11 May, with the Petronius platform easternmost in Figure 1) before heading south and southwest toward deepwater platforms. The 10 May sampling was conducted by automated instruments only; the sea was too rough for deck work. Clouds continued through 12 and 13 May. The southernmost point of the cruise was near the Atlantis platform; legs to the Brutus platform and back to the Atlantis platform followed (13 May in Figure 1). Deepwater sampling concluded with a return to Mars/Olympus (14 May), followed by the track east and north toward the Petronius platform (15 May revisit). The *R/V Point Sur* headed toward the higher-density platform region to the west, sampling on 16 May. The cruise finished with a LOOP circumnavigation (17 May in Figure 1) before returning to LUMCON in the afternoon (local time; LT) of 18 May 2019.

## 2.1. $\text{NO}_2$ Observations

### 2.1.1. OMI and TROPOMI

We use total column  $\text{NO}_2$  observations that are available once daily from OMI on the NASA Aura satellite (2004–present) and from European Space Agency (ESA)’s TROPOMI instrument (Veefkind et al., 2012) on the Sentinel-5P satellite (2018–present). Overpasses for both satellites occur early afternoon approximately between 1300 and 1400 LT. OMI operates with FOVs varying in size from  $\sim 13 \text{ km} \times 24 \text{ km}$  near nadir to  $\sim 24 \text{ km} \times 160 \text{ km}$  at the outermost edges of the swath, observing direct and back scattered solar radiation between 264 and 504 nm needed for retrieving  $\text{NO}_2$  column (total, tropospheric, and stratospheric) densities (Boersma et al., 2011; Levelt et al., 2006, 2018). NASA OMI  $\text{NO}_2$  Standard Product, V3.1 (OMNO2 product; Krotkov et al., 2017), validated in Choi et al. (2020), was available for preliminary reports on SCOAPE (Thompson, 2020; Thompson et al., 2020). The current analysis uses the new OMI V4.0 OMNO2 data described in detail in Lamsal et al. (2021). Differences between V3.1 and V4.0 OMI  $\text{NO}_2$  data include significant improvements in air mass factors (AMFs), crucial for calculating vertical column  $\text{NO}_2$  from slant column amounts, via a new surface reflectivity product and cloud retrievals for  $\text{NO}_2$ . Specifically, the V4.0 algorithm now incorporates (a) a new daily and OMI FOV specific geometry-dependent surface Lambertian Equivalent Reflectivity product in both  $\text{NO}_2$  and cloud retrievals; (b) improved cloud parameters from a new cloud algorithm (OMCDO2N) that are retrieved consistently with  $\text{NO}_2$ ; and (c) a more accurate terrain pressure calculated using OMI ground pixel-averaged terrain height and monthly mean Global Modeling Initiative terrain pressure. This product contains total, stratospheric, and tropospheric  $\text{NO}_2$  vertical column densities and is available at [https://disc.gsfc.nasa.gov/datasets/OMNO2\\_V003/summary/](https://disc.gsfc.nasa.gov/datasets/OMNO2_V003/summary/). Both V3.1 and V4.0 versions of OMI  $\text{NO}_2$  column data are presented in this work using OMI pixels with effective cloud fraction less than 30% and quality flags indicating good data for comparisons in the GOM land–water interface.

The TROPOMI  $\text{NO}_2$  algorithm (van Geffen et al., 2022 and references therein) uses a three-step approach, initially used for the Dutch OMI  $\text{NO}_2$  product (DOMINO; Boersma et al., 2007), starting with the DOAS method that determines the slant column density with spectral information from the visible band (400–496 nm) as described by van Geffen et al. (2018). Individual TROPOMI  $\text{NO}_2$  column ground pixels are 7.2 km in the along-track and 3.6 km in the across-track direction at nadir ( $\sim 14 \text{ km}$  wide at the edge of swath). The latest TROPOMI  $\text{NO}_2$  algorithm improvements are described in van Geffen et al. (2022) including differences between v1.3 and the latest v2.1/2.2 data products. During the SCOAPE cruise and the period of the current analysis, only v1.3 offline data were available at the ESA public data hub (<https://s5phub.copernicus.eu/>) so those measurements are used in this study. (We were able to compare the Sentinel-5P Product Algorithm Laboratory [S5P-PAL] TROPOMI data set, which uses a newer  $\text{NO}_2$  operational processor [version 2.3.1] with the currently available Level 1B radiances. Differences between the S5P-PAL and v1.3 data over the GOM were typically  $<5\%$ .) The TROPOMI v1.3  $\text{NO}_2$  product includes a combined quality assurance value (qa\_value) enabling end users to easily filter data. The recommended qa\_value  $> 0.75$  to eliminate cloudy scenes and problematic retrievals was applied to the TROPOMI observations presented below.

**Table 2**  
*Offshore Instrumentation on R/V Point Sur During SCOAPE Cruise*

Species	Instrument	Collaborator
NO <sub>2</sub> (and calibrator)	In situ (Teledyne API T500U CAPS)	NASA GSFC
Column NO <sub>2</sub>	Pandora	NASA GSFC (Swap <sup>a</sup> )
O <sub>3</sub>	In situ (Thermo Fisher Scientific 49i UV Photometer) and Ozonesondes	NASA GSFC
Temperature, RH, pressure, wind	Met system (Vaisala all-in one meteorological sensor)	R/V Point Sur
Aerosol (AOD) and O <sub>3</sub> columns	Microtops Columns	NASA GSFC
VOC (plus CO and CH <sub>4</sub> )	In situ canisters	UCI (Blake)
PBL height	Ceilometer (Lufft CHM 8k)	UMBC (Delgado)
Black carbon	Aethalometer (Magee Scientific RTA10 7-channel)	NIST (Conny)
CH <sub>4</sub> , CO <sub>2</sub> , H <sub>2</sub> O	In situ (Picarro G-1301m)	GSFC (Kawa/Hanisco)

<sup>a</sup>Collaborators for loaned instruments in parentheses.

### 2.1.2. In Situ Analyzers and the Pandora Spectrometer Instrument

Surface NO<sub>2</sub> mixing ratios were measured by two Teledyne API T500U Cavity Attenuated Phase Shift (CAPS) NO<sub>2</sub> instruments (Kebabian et al., 2005). For a month prior to the cruise as well as during the cruise, one CAPS instrument was situated at the LUMCON building as a reference for the three Pandora spectrometers being tested on the roof. The second CAPS instrument was installed in the portable climate-controlled trailer on the R/V Point Sur with other in situ instruments (Tables 2 and 3). The trailer was situated on the main deck forward of the ship's exhaust stack to avoid contamination. Air was sampled via a VACUUBRAND ME1 Diaphragm Vacuum Pump and introduced into the instruments with a ~5 m sampling line. Air for the trailer instruments was drawn from a common inlet ~5 m above the ship's bow deck, that is, approximately 10 m above the water surface. All continuous in situ measurements were recorded at 1-min intervals.

The only instrument requiring calibration during the cruise was the T500U CAPS NO<sub>2</sub> monitor which gave consistently high-quality data. It was first calibrated on the ship on 9 May before sailing from LUMCON. The instrument was fed zero air and measured +0.072 ppbv. The instrument was calibrated to zero. One hundred ppbv NO<sub>2</sub> using the Serinus Cal 2000 gas calibrator and an EPA Protocol gas calibration cylinder was then fed into the instrument, and it read 98 ppbv (calibrated to 100 ppbv). After the cruise, this same single-point calibration was performed again on the ship on 18 May. The zero read −0.06 ppbv, and the 100 ppbv level read 100.5 ppbv. A correction to the zero level was applied to account for a small drift from 0.00 to −0.06 ppbv over the cruise period. A correction to the 100 ppbv level was therefore not necessary.

The Pandora instrument is a ground-based UV–VIS spectroscopic instrument that provides high spectral and temporal resolution measurements of various trace gases (Herman et al., 2009). In order to retrieve columnar trace gas amounts, spectra are analyzed using the DOAS technique (Platt & Stutz, 2008). Spectral measurements can be made using direct-sun/lunar (DOAS) and sky scan (Multi-Axis DOAS, MAX-DOAS) measurement modes to retrieve trace gas columns and profiles, respectively. Direct-sun measurements were made during SCOAPE to ensure high temporal resolution and lower AMF uncertainties, allowing for more rigorous comparisons with space-based remote sensing measurements. The integration time was variable during each day based on the

**Table 3**  
*Onshore Instrumentation During SCOAPE Cruise*

Species	Instrument	Collaborator
NO <sub>2</sub>	In situ analyzer (Teledyne API T500U CAPS)	NASA GSFC (Sullivan)
NO <sub>2</sub>	Mobile in situ (NO <sub>2</sub> sonde)	KNMI (Stein-Zweers/den Hoed)
Column NO <sub>2</sub>	Pandora	NASA GSFC (Swap)
VOCs (plus CO and CH <sub>4</sub> )	In situ canisters	UCI (Blake)
PBL height	Ceilometer (Vaisala CL31)	U Houston (Flynn)



measurement schedule design. During the beginning and end of the day, the integration time ranged between 2 and 5 ms. During the majority of daylight hours, the integration time ranged between 10 and 15 ms.

Standard Pandora data products, total column  $O_3$  and  $NO_2$ , were all processed using BlickP v1.7.16. Total column  $NO_2$  measurements, which are used in this work, have an accuracy of 0.05 DU ( $2.7 \times 10^{15}$  molec-cm $^{-2}$ ; Luftblick, 2021). All data were filtered using the L2 data quality flags to include only data with high (0 or 10) or medium quality (1 or 11; Luftblick, 2019a, 2019b). Pandora TC  $NO_2$  observations were resampled to 5-min averages for comparison to other measurements.

The three NASA Pandora instruments deployed for SCOAPE featured the latest hardware and software upgrades available at that time (Luftblick, 2021, 2022). Each of these Pandoras (designated as P66, P67, and P68) were assembled at the same time with the most up-to-date instrument computer (Cincoze DC-1100), internal electronics (e.g., relay board, microcontroller), and tracker (LuftBlick TR1). Compared to the original tracker, the new Pandora tracker responds faster, has smoother movements, higher range of motion, and updated software for monitoring of the absolute position (Luftblick, 2019a, 2019b). The advanced tracker also allows integration of a head sensor camera, enabling accurate sun tracking on a moving platform, a feature that was crucial to making high-quality column measurements onboard the *R/V Point Sur*. These data could be directly compared to satellite measurements.

In addition to the three Pandoras having similar hardware and software, the calibration approach was standardized for the instruments. Field calibration, which is necessary for accurate retrievals of total column  $NO_2$ , requires obtaining reference spectra from actual field measurements for each Pandora instrument. While the three Pandoras were collocated at LUMCON (Cocodrie, LA) for 4 weeks prior to P66 being deployed to the *R/V Point Sur*, reference spectra for performing the Minimum Langley Extrapolation (MLE) were selected for each instrument using data collected between 17:55:00 UTC and 18:05:00 UTC on 20 April 2019 when all three instruments sampled clear skies and low tropospheric  $NO_2$  amounts. A larger range of data (19 days) was then selected, including the date of our reference spectra, as we assume there is a subset of data in the data series that is independent of AMF. The slope of the red lines on the MLE (Figure S1 in Supporting Information S1) indicates the minimum vertical column at that location, which should be approximately the stratospheric column. This intercept is equal to our slant column reference amount, which can be added to all the slant column data to produce absolute slant columns and eventually divided by the AMF to produce vertical column amounts. There can be variability in the exact slant column reference amount between instruments; however, overall, there was good consistency in the slant column reference amounts among the three instruments (Figure S2 in Supporting Information S1; data taken from NASA/LARC/SD/ASDC [2022c]). This rigorous field calibration ensured consistency among instruments and led to very good agreement as shown in Figure S2 in Supporting Information S1. Time-matched data from P66, P67, and P68 show the reproducibility of the three Pandora instruments during the 4-week LUMCON test period, as illustrated by referencing Pandoras 66 and 68 to Pandora 67. Agreement in terms of slope and offset of the best fit lines, as shown in the lower right box in Figure S2 in Supporting Information S1, is excellent. The correlation coefficient,  $R$ , is lower for Pandora 66 because, as the blue symbols show, the latter instrument is slightly noisier than the other two. Figure S3 in Supporting Information S1 displays comparisons of the three Pandora instruments inclusive of the precruise period along with Pandoras 67 and 68 that remained at LUMCON during the cruise period. Overpass comparisons for TROPOMI (gold diamonds) and OMI (magenta triangles) are also shown. Mean Pandora-TROPOMI TC  $NO_2$  offsets are  $\sim 13\%$  (Figure S3 in Supporting Information S1), with the Pandora measuring higher column amounts than TROPOMI. There is more scatter among the three Pandoras during a cloudy period before the cruise on 4–8 May 2019 (Figure S2 in Supporting Information S1).

## 2.2. Other Surface-Based Observations

Routine meteorological parameters (temperature, relative humidity, and winds), which were provided by the *Point Sur*, and continuous  $NO_2$ ,  $O_3$ ,  $CH_4$ , and  $CO_2$  data were collected during SCOAPE (Table 2). We averaged all in situ  $NO_2$  observations to 5-min to match the 5-min Pandora averages. Uncertainties for these instruments specified in Martins et al. (2016) and Kollonige et al. (2018) are 5% for  $NO_2$  and 1.3% for  $O_3$ . Surface  $NO_2$  and Pandora TC  $NO_2$  spikes that were obviously caused by sampling of the *Point Sur* exhaust were removed from analyzed data as follows. Plume\_flag\_1 in the SCOAPE data archive marks times when relative winds were from 135° to 225° (blowing from exhaust stack to front of ship) and relative wind speeds were less than 5 m/s. Plume\_flag\_2 was chosen to eliminate coincident spikes in  $O_3$  (downward) and  $NO_2$  (upward). Analyses of authentic  $NO_2$  spikes are presented in Section 3.3.



Whole-air, evacuated stainless steel canisters for a large suite of VOC species, CH<sub>4</sub>, and CO measurements were filled 2–3 times each day on the *Point Sur* for postcruise analyses. They were analyzed by the Rowland-Blake research group (Colman et al., 2001) for a range of alkanes, alkenes, aromatics, halogenated carbon species, CO, CH<sub>4</sub>, dimethylsulfide (DMS), and other trace gases. Because of the real-time CO analyzer failure, we report CO data from the flasks only. Subsamples of each canister were transferred via vacuum line to 12 mL evacuated glass vials for stable isotope analysis ( $\delta^{13}\text{C}$  and  $\delta\text{D}$ ) via isotope ratio mass spectrometry (IRMS) at the University of Cincinnati via the method of Yarnes (2013). The IRMS instrument is calibrated several times daily with standards bracketing the isotopic composition of samples and with standards matched to the concentration of samples to avoid linearity issues. The reproducibility of  $\delta^{13}\text{C}$  and  $\delta\text{D}$  is 0.2‰ and 4‰, respectively.

Flask sampling on the *R/V Point Sur* was normally coordinated with a platform encounter. For large platforms, when a plume downwind was intercepted, as denoted by simultaneous NO<sub>2</sub> and CO<sub>2</sub> spikes, a flask was exposed to collect an air sample. The platform was circled and the process repeated to get an upwind sample. For smaller operations closer to shore (10–11 May and 16–17 May in Figure 1), plumes were more frequent and maneuvers for contrast sampling were not practical. When the *R/V Point Sur* was near shore a number of flask collections were coordinated with flask fillings on land, 11–17 May, for example, at Venice, Port Fourchon and other sites shown by red pins in Figure 1. Several flasks were filled during a circling of the LOOP on 17/18 May.

Boundary-layer information was supplied by Internet-1-RSB radiosondes launched once or twice daily from 11 to 17 May. In most cases, En-Sci electrochemical concentration cell ozonesondes were launched with the radiosondes; the ozonesonde sensing solution was the 0.5% KI, half-buffer variant (Thompson, Smit, et al., 2019). The nominal launch time was midday, near the OMI and TROPOMI overpass time. On 4 days of the cruise, 14 May, 15 May, 16 May, and 17 May, ozonesondes were also launched earlier in the day when the boundary-layer height was near its daily minimum as indicated by the shipboard ceilometer (Tables 2 and 3).

### 2.3. Meteorological Forecasts, Reanalysis, and Trajectories

To monitor the meteorological conditions throughout the cruise, the Goddard Modeling and Assimilation Office (GMAO) provided near-real-time support ([https://gmao.gsfc.nasa.gov/field\\_campaigns/past\\_campaigns](https://gmao.gsfc.nasa.gov/field_campaigns/past_campaigns)) with weather forecasts and data assimilation products from Global Earth Observing System (GEOS)-Forward Processing (GEOS-FP; <https://fluid.nccs.nasa.gov/weather/>) and composition forecasts with their GEOS-Composition Forecasts (GEOS-CF) products (<https://fluid.nccs.nasa.gov/cf/>). Both the FP and CF products were used in making fine adjustments to the cruise track as they indicated two different meteorological regimes while the *Point Sur* was sampling.

Postanalysis used the Modern-Era Retrospective analysis for Research and Applications Version 2 (MERRA-2) reanalysis, which is driven by the GEOS-5 atmospheric data assimilation system with  $1/2^\circ \times 2/3^\circ$  resolution and 72 layers, to demonstrate the large-scale changes in meteorological conditions during the SCOAPE cruise and the impact on the *R/V Point Sur* in transit (Section 3.1). To trace source regions for air arriving at the *R/V Point Sur*, we initialized 12-hr ensemble back trajectories using the Hybrid Single-Particle Lagrangian Integrated Trajectory model (HYSPPLIT; <https://www.arl.noaa.gov/hysplit/>) developed by NOAA's Air Resources Laboratory (Stein et al., 2015), driven by National Centers of Environmental Prediction (NCEP) Global Data Assimilation System (GDAS) meteorology every 3 hr at  $0.5^\circ$  resolution at 50 and 500 m above sea level (Section 3.2.3).

## 3. Results and Discussion

### 3.1. Meteorological Overview of Two Regimes: Marine and Continental Air Masses

The GOM study region during the cruise period of 10–18 May 2019 was characterized by two distinct meteorological regimes. These consisted of primarily onshore (10–13/14 May; “marine”) and offshore (14–18 May; “continental”) flow that led to contrasts in the chemical composition. The change in large-scale conditions originated from a weak frontal system that drifted northwest to southeast through the GOM during the middle of the cruise. The progression of the frontal system is presented in Figure 2, with MERRA-2 reanalysis mean sea-level pressure (MSLP; black contours), 1,000 hPa wind vectors (arrows), and specific humidity ( $q$ ; colors) shown for 12 UTC (06 LST; the *Point Sur* position is the red dot). The entire 10–18 May SCOAPE track is overlaid in cyan.

The onshore flow “marine” period dominated the first few days of the cruise with easterly to southerly winds and high humidity. The 12 and 13 May snapshots in Figures 2a and 2b display the contrast in wind direction and speed, and humidity along the frontal boundary. The event was analyzed as a cold front by NOAA's Weather

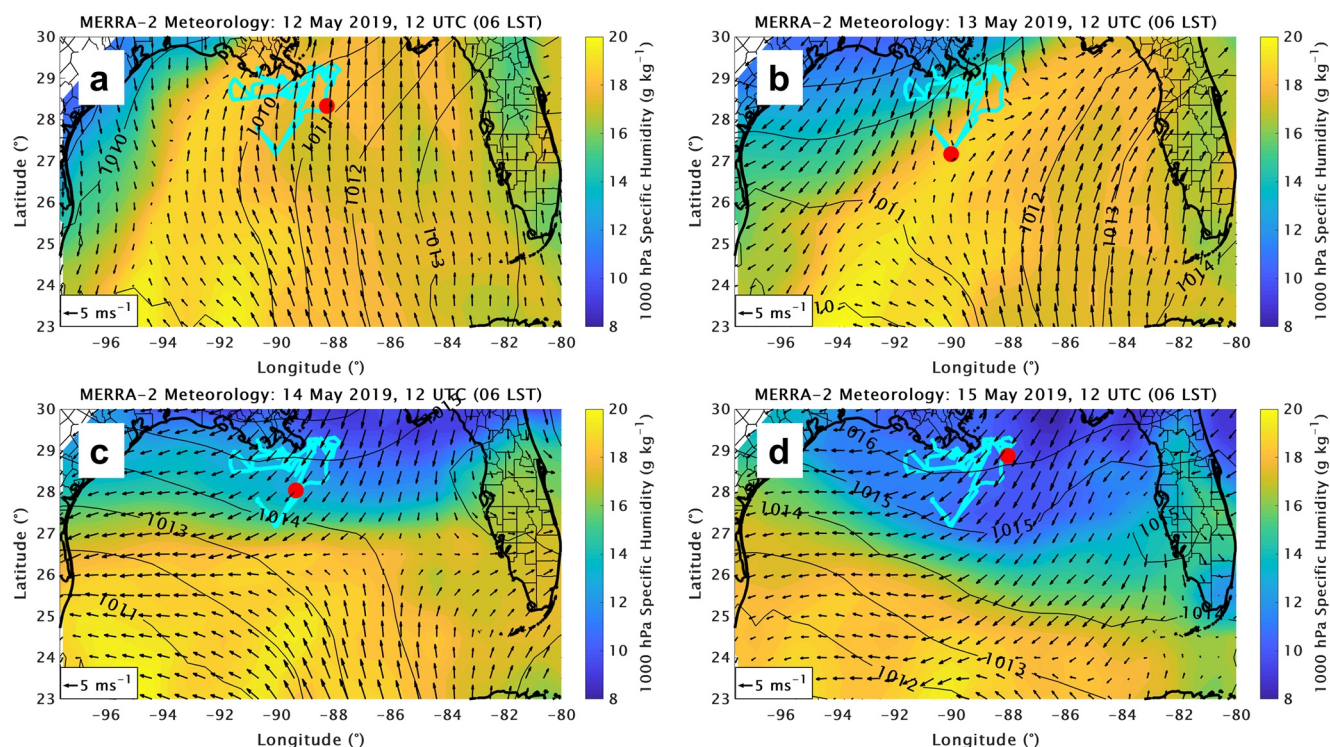


**Figure 2.** MERRA-2 meteorological reanalysis at 12 UTC (0600 local time) for 4 days (12–15 May 2019) that capture the transition from onshore flow (a, b), to mostly offshore winds (c, d). Unpolluted, moister tropical air masses were sampled on 12 and 13 May with a transition to air parcels originating from the near-shore and more urban Louisiana coastal areas on 14 and 15 May. The *R/V Point Sur* cruise track is shown in cyan, with the location of the ship indicated by the red dot. MERRA-2 MSLP (black contours), 1,000 hPa wind vectors (black arrows), and 1,000 hPa specific humidity (colors) summarize the large-scale meteorological conditions encountered during the middle of the cruise.

Prediction Center ([https://www.wpc.ncep.noaa.gov/archives/web\\_pages/sfc/sfc\\_archive\\_maps.php?arcdte=05/13/2019&selmap=2019051312&maptype=namussfc](https://www.wpc.ncep.noaa.gov/archives/web_pages/sfc/sfc_archive_maps.php?arcdte=05/13/2019&selmap=2019051312&maptype=namussfc)). Specific humidity values increased by nearly a factor of 2 from northwest ( $\sim 10 \text{ g kg}^{-1}$ ) to southeast ( $\sim 20 \text{ g kg}^{-1}$ ), with a corresponding change in the wind direction/source region across the front. On 13 May, the *Point Sur* (red dot on Figure 2b) sat in a transition zone along the front and in between the two distinct air masses. After 13 May, the frontal boundary pushed farther southeast into the GOM, and the wind direction became northeasterly/easterly (Figures 2c and 2d), with trace gas measurements from the ship and satellite data indicating sources from more polluted, “continental” regions. Detailed analyses of the effects of the two large-scale meteorological regimes on the cruise pollution measurements follow in Sections 3.2 and 3.3.

### 3.2. Chemical Composition in Two Regimes: Unpolluted Marine and Moderately Polluted Continental

#### 3.2.1. Satellite Views of Total Column ( $\text{TC NO}_2$ )

Satellite column data ( $\text{TC NO}_2$  in Figure 3) capture the contrast of the two regimes. Cloud cover precluded extensive retrievals over much of the open GOM on 13 and 15 May for OMI (Figures 3a and 3b). Both OMI and TROPOMI measurements for 13 May displayed relatively low levels of  $\text{TC NO}_2$  except for values of  $\text{TC NO}_2 > 0.20 \text{ DU}$  over the New Orleans and Baton Rouge areas (red and orange in Figures 3c and 3e). For 15 May, after the wind shift brought continental air offshore (Figures 2c and 2d) and cloud cover retreated (mostly  $< 0.1$ , Figure 3b), the urban regions and the adjacent GOM registered widespread pixels with readings exceeding  $0.15 \text{ DU TC NO}_2$  (Figures 3d and 3f). The satellite maps in Figure 3 display overall OMI and TROPOMI similarities but detailed comparison of  $\text{TC NO}_2$  also highlights some differences, the horizontal resolution of the two sensors being the most obvious. Individual orange-to-red pixels recorded by TROPOMI on 15 May (Figure 3f) may indicate  $\text{NO}_x$  sources over land and the adjacent GOM where small platforms are concentrated (Figure 1). However, TROPOMI retrievals run  $\sim (0.03\text{--}0.05) \text{ DU}$  greater than the corresponding  $\text{TC NO}_2$  OMI readings, primarily along the coast but also over GOM between  $27.0^\circ\text{N}$  and  $28.5^\circ\text{N}$  latitude. These differences are evaluated with the



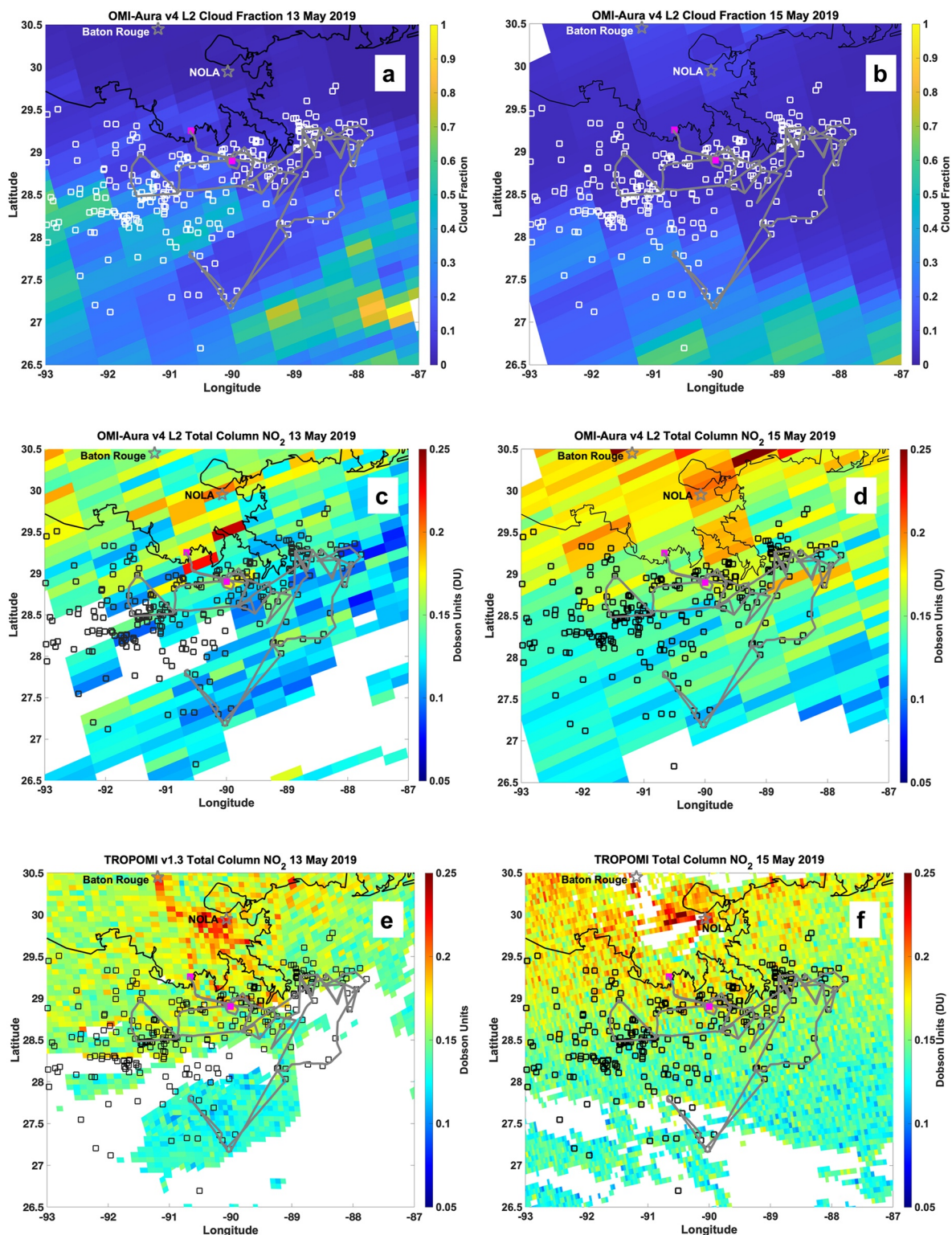


**Figure 3.** OMI v4 effective cloud fraction over SCOAPE cruise region on (a) 13 May 2019 and (b) 15 May 2019 (Krotkov et al., 2019). Total column (TC)  $\text{NO}_2$  (DU) over SCOAPE cruise region from OMI v4 on (c) 13 May 2019 and (d) 15 May 2019 (Krotkov et al., 2019). TROPOMI v1.3 TC  $\text{NO}_2$  (DU) for (e) 13 May 2019 and (f) 15 May 2019 (Copernicus Sentinel-5P, 2018). TROPOMI maps produced using the PAL retrieval for May 2019 differed from TROPOMI v1.3 by < 5% overwater. In (c)–(f), black open squares are the locations of the top 500  $\text{NO}_x$ -emitting platforms from BOEM's 2014 inventory (Wilson et al., 2017); white open squares mark the same in (a) and (b). The gray solid line marks the *R/V Point Sur* cruise track. New Orleans, Louisiana (NOLA), and Baton Rouge are indicated with open gray stars.

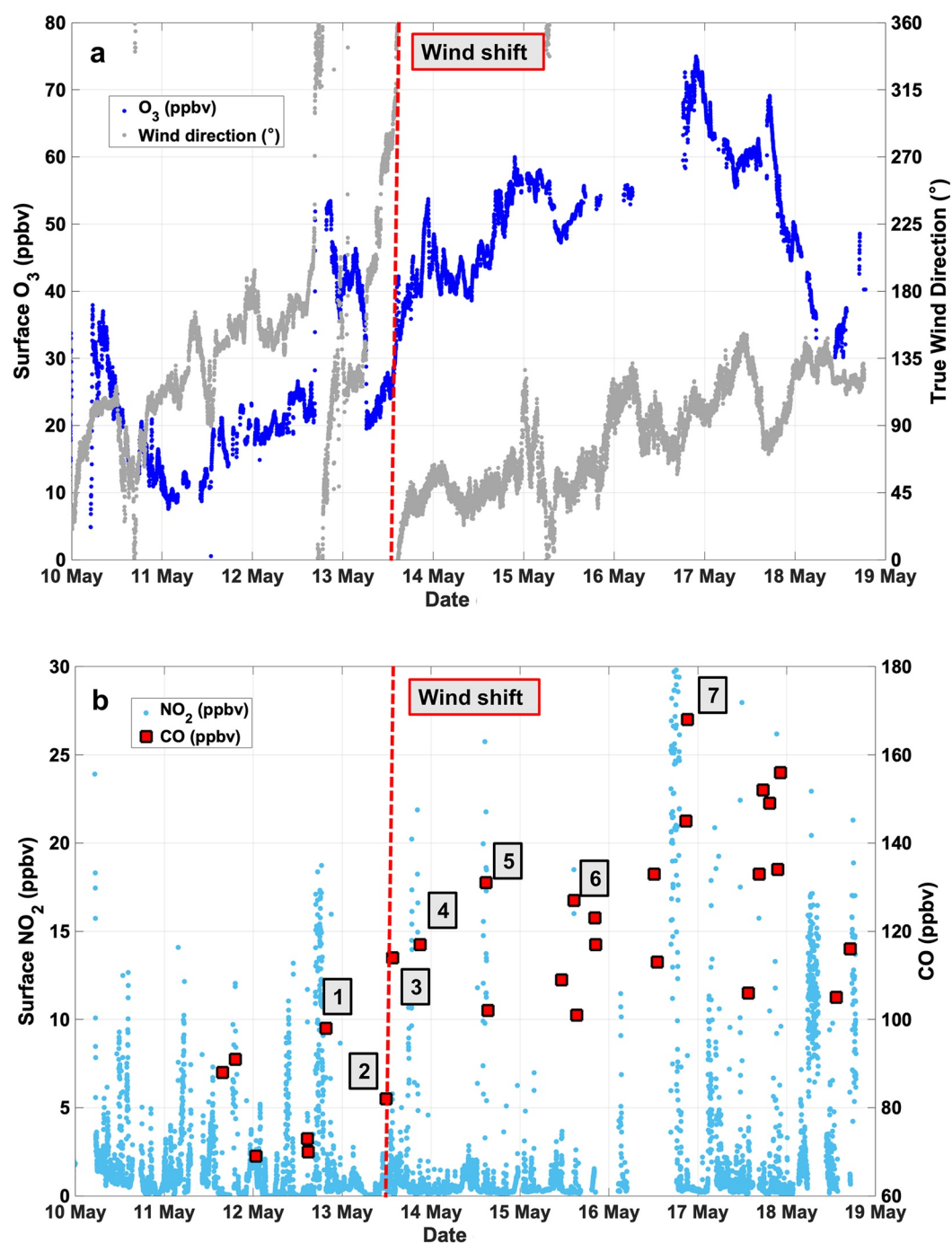


**Figure 4.** (a) Ozone mixing ratio (left scale) in ppbv with wind direction (right scale, in °) measured on *R/V Point Sur* during May 2019 cruise (presented as 5-min means); (b) NO<sub>2</sub> mixing ratio (left scale; 5-min means) in ppbv with CO mixing ratio in ppbv from canister samples taken along the *Point Sur* track. Trace gas data retrieved from NASA/LARC/SD/ASDC (2022d). Sampling locations (Figure 1) are as follows: 1 = vicinity of Mars/Olympus deepwater platform complex; 2 = near Atlantis platform before 13 May wind shift (Figure 2); 3 = between Marco Polo and Shenzi platforms after 13 May wind shift; 4 = near Brutus platform, volatile organic compound (VOC)-enriched plume detected; 5 = second encounter, vicinity of Mars/Olympus complex, 14 May, plume detected. Note: surface NO<sub>2</sub> values are higher than encounter (1) because the background is more polluted on 14 May than on 12 May; 6 = near Petronius, second encounter (see elevated methane, VOC in Figure 7, also Figures 9 and 10a); 7 = surrounded by numerous shallow-water platforms in western area, where VOC-enhanced plume detected (Table 4).



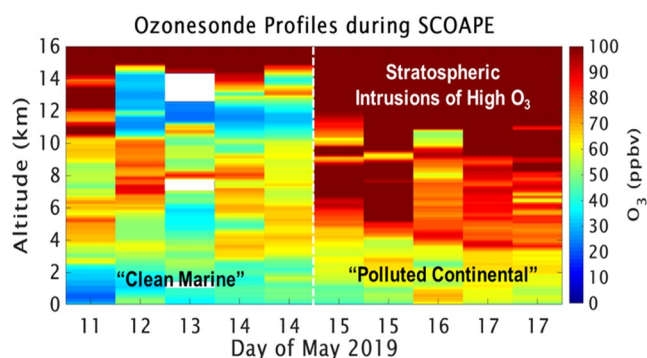


**Figure 5.** Ozonesonde profiles during SCOAPE, data downloaded from NASA/LARC/SD/ASDC (2022a). Mixing ratios to 16 km are illustrated. Blue colors are concentrations associated with tropical marine boundary layer. On 12–14 May, ozone concentrations 20–30 ppbv above 10 km are typical of air parcels in which deep convection introduced boundary-layer air. From 15 to 17 May, layers with >80 ppbv signify stratospheric influence. See Figure S7 in Supporting Information S1 where up to 14 May lower ozone mixing ratios occur with higher humidity measured by the accompanying radiosondes. From 15 to 17 May, from 4 to 16 km, the median relative humidity has fallen to <10%.

shipboard Pandora 66 (P66) and the two Pandoras (P67, P68) at LUMCON (Section 3.3.3).

Not all  $\text{NO}_2$  pollution observed by satellites and on the *R/V Point Sur* during the transition of air masses on 13–14 May was from the nearby region. Starting on 13 May, the cruise encountered air originating from Mexican agricultural fires upwind of the ship. Figure S4 in Supporting Information S1 shows elevated MODerate resolution Imaging Spectrometer (MODIS) aerosol optical depth (AOD; Naval Research Laboratory and the University of North Dakota/MODIS Adaptive Processing System [MODAPS], 2017) as dark reds in false color transported northward into the SCOAPE cruise region from areas of concentrated fire counts derived from MODIS and Suomi National Polar-Orbiting Partnership (Suomi NPP) Visible Infrared Imaging Radiometer Suite (VIIRS; Giglio & Justice, 2021; Schroeder & Giglio, 2017) observations (orange and red dots in Mexico). The Atmospheric Infrared Sounder (AIRS; AIRS Science Team/Joao Teixeira, 2013) captured elevated midtropospheric CO plumes from Mexico in the vicinity of the SCOAPE cruise on 13–14 May (Figure S5 in Supporting Information S1). Precise  $\text{NO}_2$  source attribution is beyond the scope of this study, but we note that the GEOS-CF model forecast used during the cruise identified a CO-fire tracer originating from Mexico over the SCOAPE sampling region on 14 May (not shown).

### 3.2.2. Shipboard Measurements of Ozone and Other Trace Gases

The switch from clean marine air to a more continental influence is reflected in a number of constituents. Figure 4a shows that late on 13 May there was an abrupt transition in wind direction (gray line) measured on the ship from mostly south/southwest to north/northeast. Surface ozone (blue line) increased from 20 ppbv or less to more than 40 ppbv, with peak readings of >70 ppbv on 16–17 May (note back trajectories from ship location on 15 and 17 May, Figure S6 in Supporting Information S1). The lowest ozone values measured at the beginning of the cruise, 10–13 May 2019, are referred to as having air of “marine” origins (Figure 2). After 13 May, the air is designated as “continental” with the high-ozone levels on the last days occurring in the westernmost segment of the track (Figure 1). Surface CO from shipboard canister samples (Figure 4b) also reflects the marine versus continental classification. Prior to 13 May, CO mixing ratios from seven measurements range from 55 to 95 ppbv, levels associated with the equatorial Atlantic (Thompson et al., 2000). After 13 May, the canister samples range from 100 to 170 ppbv CO, with a mean value of ~130 ppbv for the period 14–18 May. Daily CO mixing ratios from the canister samples (Figure 4b) abruptly changed from “marine” values of ~80 to ~120 ppbv on 13 May, when the *Point Sur* encountered air parcels from the Mexican fires. Mixing ratios of CO remain elevated on 14 May when an aerosol plume from the fires was transported to the *Point Sur* (Figure S4b in Supporting Information S1). AIRS CO (Figure S5 in Supporting Information S1) shows a similar movement of fire pollution from 13 to 14 May although much of the ship sampling area is obscured by clouds. Figure 4b displays shipboard surface  $\text{NO}_2$ . The overall marine versus continental contrast is present but there are many pollution spikes in the “marine” period of the cruise when the *Point Sur* was sampling near platforms, usually within 1.5–2 km (1 and 2 labels in Figure 4b; Figure 1). Elevated  $\text{NO}_2$  measurements from the ship analyzer were found between Brutus and Atlantis and southwest of the Mars/Olympus platforms (labels 3–5 in Figure 4b; Figure 1).

The ozonesonde ozone mixing ratio curtain (Figure 5) captures the complex vertical structure of air passing over the *Point Sur*. During the “clean marine” phase, the sharp ozone gradient seen at 15 km on 12–14 May is typical of the tropopause in tropical air. The low-ozone layer between 10 and 14 km may originate from convective redistribution of air from the surface to cloud-outflow level (Petropavlovskikh et al., 2010; Thompson et al., 2010, 2012). The continental air, in contrast, that displays a tropopause closer to 10 km and ozone greater than 80 ppbv, is pervasive above 3 km. In addition, the midtroposphere includes ozone of stratospheric origins (note shift to very low water vapor, Figure S7 in Supporting Information S1), which is common in spring.

A snapshot of marine versus continental influences for  $\text{CH}_4$ , CO,  $\text{CO}_2$ , and DMS concentrations, based on the 27 *Point Sur* flask samples, appears in Figure 6. DMS is of marine biogenic origin, so it is greater in the first part of the cruise, up to 14 May, than in the latter part. Species with continental biogenic origin (isoprene,  $\alpha$ - and  $\beta$ -pinene, not shown) exhibit the opposite pattern. Figure 7 summarizes the relationship between ethane and

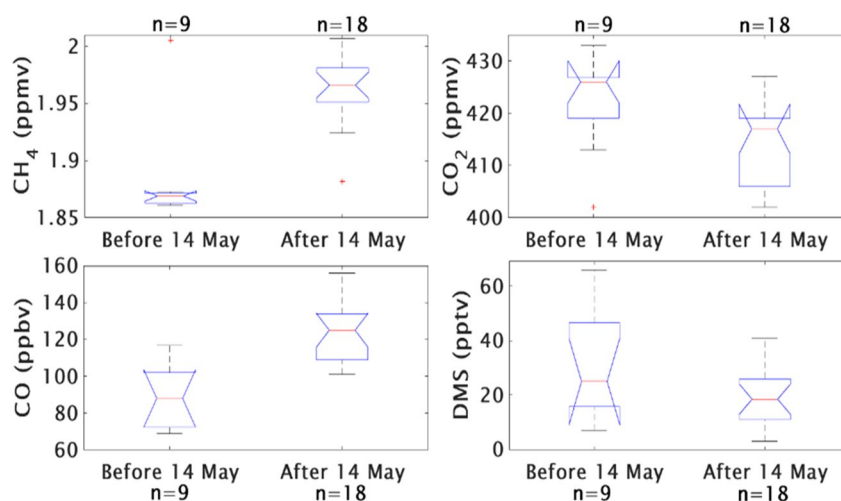


**Figure 6.** Box and whisker panels for  $\text{CH}_4$ ,  $\text{CO}$ ,  $\text{CO}_2$ , and dimethylsulfide (DMS) before (left side of each panel) and after 14 May (right side of each panel). Data were taken from NASA/LARC/SD/ASDC (2022a). Sample numbers indicated at the top or bottom of each panel. Red line denotes median values, blue box denotes 25th and 75th percentile, and whiskers (dashed bars) are 95th percentile. Notches in the boxes indicate the 95% confidence interval of the median values.

$\text{CH}_4$  as well as  $\delta^{13}\text{C}$  and  $\delta\text{D}$  for both regimes based on 15 flask samples offshore and 2 flask samples onshore. Both  $\text{CH}_4$  isotopes (Figure 7a) show small changes to more negative values during the shift from marine to more continental air (Figure 7b displays sample locations). Ratios in Figure 7 represent enhancements above mean  $\text{CH}_4$  and ethane campaign values. The highest enhancement ratios are observed after 14 May in the vicinity of the far eastern shallow and deepwater platforms (e.g., Petronius, Point 6 in Figures 4b and 7b, with moderate  $\text{CO}$  and relatively low surface  $\text{NO}_2$ ) and the far western shallow-water platforms (Figure 7b). This distribution is similar to previous limited GOM sampling, for example, Yacovitch et al. (2020). Note that the two onshore samples show more negative  $\delta^{13}\text{C}$  and  $\delta\text{D}$  compared to all the samples from the *Point Sur*.

An extreme example of air polluted with high VOC was captured in a canister sample collected near a shallow-water platform at 1612 LT Central Daylight Time (CDT) on 16 May. Figure 7a shows that an elevated  $\text{C}_2\text{H}_6/\text{CH}_4$  occurred with the most  $^{13}\text{C}$ -depleted sample. Figure 7b depicts the location of that sample in the far western region of shallow-water platforms (Point 7 in Figure 4b). Table 4 gives concentrations of representative carbon-containing compounds in the 16 May flask. The  $\text{CH}_4$  increase was a factor of  $\sim 3$  greater than the median of 27 flasks collected during the entire cruise. This concentration signified leaks from gas production; the  $\text{CO}_2$  from the same flask was nearly identical to the all-cruise  $\text{CO}_2$  flask median. However, ethane, *n*-propane, and benzene amounts were 75, 130, and 45 times higher, respectively, than their cruise averages.

### 3.2.3. Trajectory Analysis

Although the examples in Figures 4–7 illustrate considerable hour-to-hour variability in all the constituents measured, a contrast in overall AQ before and after 14 May 2019 dominates the chemical character of the GOM during SCOAPE. This is supported by air parcel trajectory analysis carried out with HYSPLIT driven by NCEP GDAS at  $0.5^\circ$  resolution. The trajectories were initialized at the start time of VOC canister sampling to help with source attribution. Figure 8 displays ensemble 12-hr back trajectories initialized at the indicated LT (CDT) 50 m above sea level (upper panels) and 500 m (lower panels) with red, green, and blue air parcels denoting a change in release time of every 3 hr over the 12-hr period. The marine regime observed by the *Point Sur* coincides with onshore flow, indicated by winds from the south-southeast on 10–12 May as shown in Figures 8a and 8d (12 May 2019 back trajectories at 0900 LT CDT) and Figure 4a in situ data. The continental regime observed after the start of 14 May indicates the wind shift from the north-northeast (Figure 4a in situ data). The corresponding trajectories appear in Figures 8c and 8f on 14 May at 1700 LT CDT. May 13 marked a transition period between these two regimes (Figure 2b). The change in wind direction viewed in Figures 8b and 8e captures the Mexican fire influence (south-west origins; cf., Figures S4 and S5 in Supporting Information S1) detected on the *Point Sur* prior to the 14 May shift to north-northeasterly winds on 14 May. Figure S6 in Supporting Information S1 provides insight into changing winds during the continental regime, 15–17 May. During that period, back trajectories show air originating

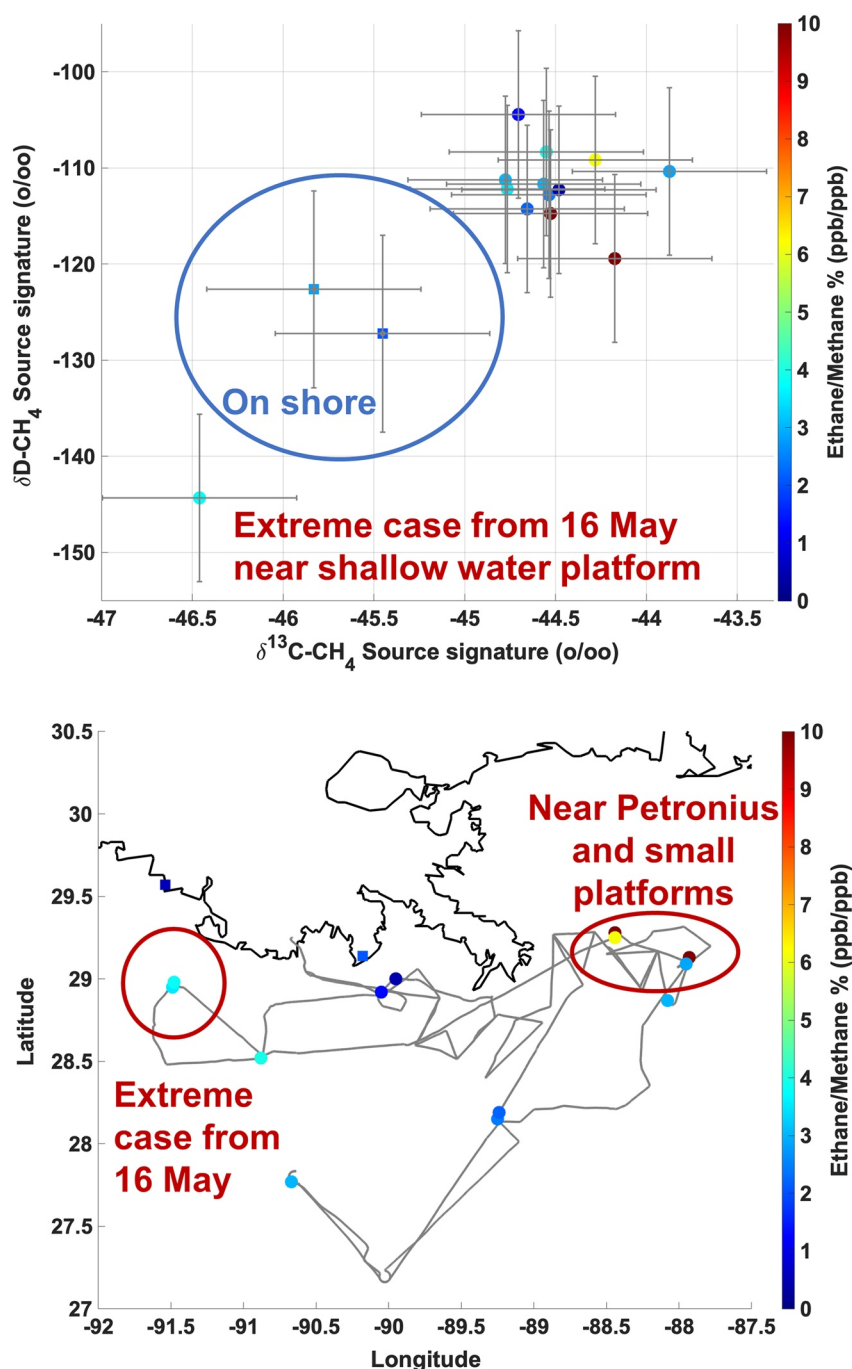


**Figure 7.** Volatile organic compound (VOC) canister observations of  $CH_4$  isotope source signatures for ship (circles) and coastal (squares) measurements 11–19 May 2019. Colormap indicates ethane to methane ratios (% (ppb/ppb)) in the scatter plot (a) and map (b). Error bars show 1-sigma standard deviation.

from along shore sources (e.g., shallow-water platforms, LOOP), as in the extreme pollution measured in the 16 May canister (Figure 7 and Table 4).

### 3.3. Satellite, Pandora, and Surface $NO_2$ During Two Regimes on SCOAPE

Figures 9 and 10 illustrate  $TC\ NO_2$  variability during the SCOAPE cruise, with observations from P66, TROPOMI, and OMI. Figure 9, that illustrates all the 5-min average P66 readings, presents a comparison of the 7 full days of SCOAPE (11–17 May). TROPOMI overpass  $TC\ NO_2$  values (diamonds for color-coded days) are also shown.



**Table 4**

*AQ Conditions From VOC Can Sample on 16 May Near Shallow-Water Platform at (28.9795°, -91.4760°)*

VOC species	Cruise median	16 May plume can	Notes
CH <sub>4</sub> (ppmv)	1.96	5.71	Deepwater platforms flare this off
CO <sub>2</sub> (ppmv)	415	418	No combustion, likely just leaky pipes
Ethane (ppbv)	2.1	145	C <sub>2</sub> H <sub>6</sub> ; second largest component of fossil gas after CH <sub>4</sub>
Propane (ppbv)	0.7	90.1	C <sub>3</sub> H <sub>8</sub> ; by-product of fossil gas processing
<i>n</i> -Butane (ppbv)	0.3	29.9	C <sub>4</sub> H <sub>10</sub> ; <i>i</i> -butane had similar concentrations
Benzene (ppbv)	0.04	1.88	C <sub>6</sub> H <sub>6</sub> ; known carcinogen

Transient spikes in P66 TC NO<sub>2</sub> are more prevalent after the wind shift on 13 May (note the transition to higher TC NO<sub>2</sub> values on 14 May in the green circles after 1800 LT, Figure 9). These signify an encounter with a local NO<sub>2</sub> source, presumably corresponding to label 5 where the *Point Sur* had its second encounter with the Mars/Olympus complex. At the same time, label 5 in Figure 4b shows that flask CO rose to 130 ppbv and the surface NO<sub>2</sub> analyzer measured more than 20 ppbv. Most of the P66 TC NO<sub>2</sub> observations on 11–13 May (red-orange, gold, and purple circles in Figure 9) are below 0.18 DU and no individual data point exceeds 0.20 DU. Where label 1 appears (gold circles, at the first pass of Mars/Olympus complex) surface NO<sub>2</sub> spikes to >10 ppbv but CO is only moderately elevated (100 ppbv in Figure 4b). After the shift to offshore winds, in contrast, from 15 to 17 May, except for ~0700, all P66 TC NO<sub>2</sub> readings are above 0.18 DU with most transient spikes displaying TC NO<sub>2</sub> > 0.22 DU. There is no consistent diurnal variation across the days although the proportion of spikes is greater early in the day on 15–17 May (dark red and blue circles in Figure 9) when the ship was near shore near a high density of platforms. An exception was near Petronius (label 6 in Figure 9). Tracers of pollution do not always correlate. Figure 4b (label 6) shows moderately elevated CO near the large Petronius platform and greatly enhanced ethane/CH<sub>4</sub> (easternmost point in Figure 7b). However, label 6 in Figure 4b shows that surface NO<sub>2</sub> was <5 ppbv. Petronius is not far from shore and a high density of smaller platforms. The Pandora may be responding to pollution layers aloft from the latter source; that would also be consistent with elevated VOC from leakage.

There were five TROPOMI overpass columns (diamonds in Figure 9) during the cruise, two on 11 and 13 May 2019 (orange-red and purple diamonds), that agreed within 0.03 DU of the coincident P66 TC NO<sub>2</sub> values. The

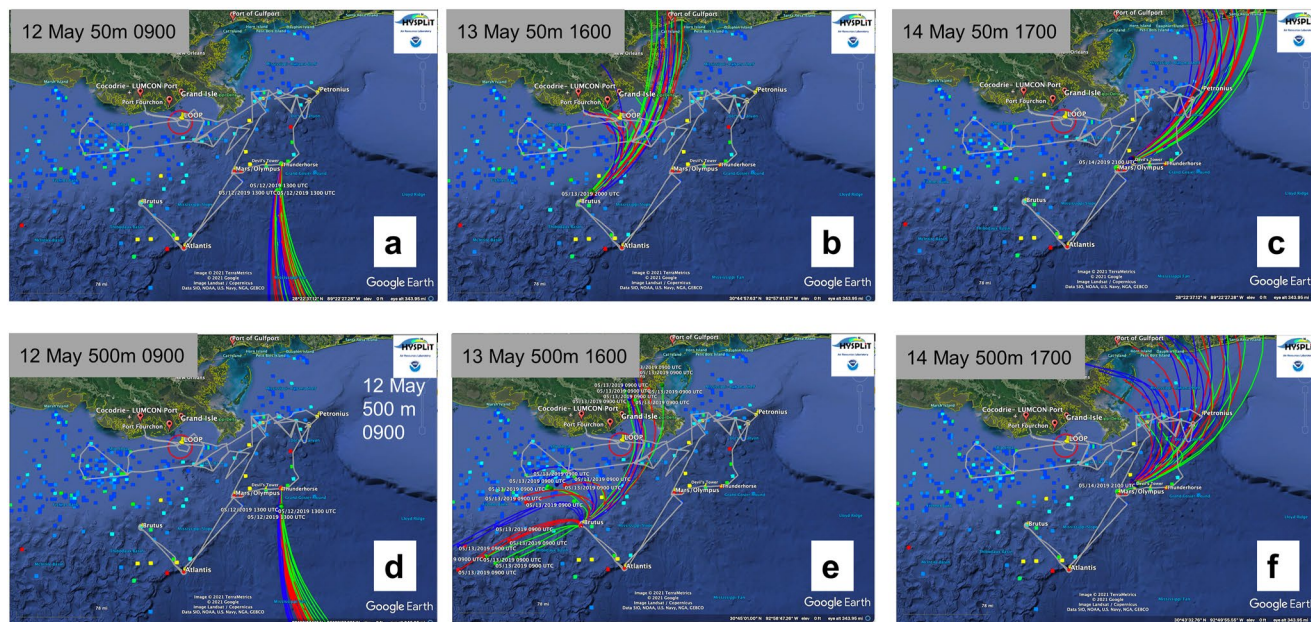


**Figure 8.** HYSPLIT 12-hr ensemble back trajectories (Stein et al., 2015) released at 50 m (top panels; a–c) and 500 m (lower panels; d–f) at the local times listed in each (12–14 May 2019) and driven by the NCEP Global Data Assimilation System (GDAS) at 0.5° resolution. Colors of the trajectories denote change in ensemble trajectories' release time (every 3 hr over 12-hr period).



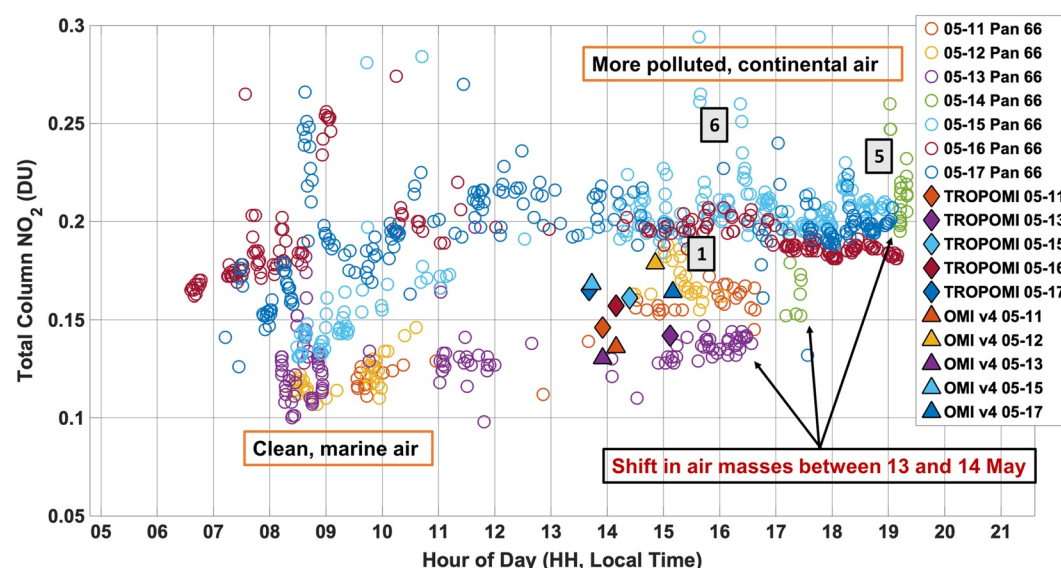


**Figure 9.** Pandora diurnal cycle of TC  $\text{NO}_2$  (data from NASA/LARC/SD/ASDC, 2022c) during the cruise period 11–17 May 2019 (color of lines denotes day of observation) with TROPOMI overpass values (diamonds in corresponding day of cruise color; Copernicus Sentinel-5P, 2018) and OMI v4 overpass values (triangles in corresponding day of cruise color; Krotkov et al., 2019). Platform encounters labeled 1, 5, and 6, as described in Figure 4. Note that although 1 (12 May) and 5 (14 May) both correspond to sampling near the Mars/Olympus complex, TC  $\text{NO}_2$  is lower for the earlier encounter because the background air with air parcels from the south (Figures 8a and 8d) is less polluted than with flows from the north and east (Figures 8c and 8f).

triangles in Figure 9 signify OMI readings for 11, 12, and 13 May 2019. The 11 and 13 May OMI TC  $\text{NO}_2$  values (orange-red and purple triangles) are 0.02–0.03 DU lower than their TROPOMI counterparts; this is very good agreement considering the different resolution of the two satellite instruments. On 12 May, near the overpass time, 1450 local, both P66 and OMI (gold triangle) measured 0.16–0.18 DU; there was not a TROPOMI observation that day. The three TROPOMI readings on 15–17 May give TC  $\text{NO}_2 \sim 0.16$  DU compared to P66 TC  $\text{NO}_2$  values  $\sim 0.20$  DU. The OMI TC  $\text{NO}_2$  readings for 15 and 17 May are 0.17 DU, virtually the same as for TROPOMI. For both OMI and TROPOMI during the 15–17 May period, the satellite TC  $\text{NO}_2$  measurements are  $\sim 20\%$  lower than those of the Pandora.

Figure 10a compares P66 and satellite TC  $\text{NO}_2$  with in situ  $\text{NO}_2$  observations during the cruise. The overall underestimate of OMI and TROPOMI satellite columns relative to P66 on 15–17 May (cf., Figure 9) is striking. The in situ  $\text{NO}_2$  values roughly follow the two-regime pattern, with surface  $\text{NO}_2$  increasing  $\sim 50\%$  after 14 May. However, most individual surface  $\text{NO}_2$  spikes during plume encounters are not detected simultaneously by the Pandora. Figure 10a shows that P66 may observe elevated TC  $\text{NO}_2$  in advance of an in situ  $\text{NO}_2$  spike on the *Point Sur* (e.g., labels 1, 4, and 7) but label 5 is the opposite. For label 6 (near Petronius, Figures 4b and 9), the high P66 measurements are not reflected in the shipboard  $\text{NO}_2$  readings. Decoupling between ambient and column  $\text{NO}_2$  can occur when the boundary layer is not well mixed, that is, high  $\text{NO}_2$  trapped near the surface may not be observed in the Pandora column. Mismatches can also result when much of the  $\text{NO}_2$  column is an above-mixed-layer residual or is advected from upwind (Thompson, Stauffer, et al., 2019). Figure 10a illustrates the complexity of surface–TC  $\text{NO}_2$  relationships. For example, 15 May is the day with the greatest range in TC  $\text{NO}_2$  values (cf., Figure 9, label 6 and paler blue circles throughout the day). There is a slow increase in P66 TC  $\text{NO}_2$  during the morning hours (before the overpass symbols) with a few ship  $\text{NO}_2$  spikes less than 5 ppbv (Figure 10a). The P66 TC  $\text{NO}_2$  readings are in a range  $(0.17 \pm 0.02)$  DU except for four green dots, three of them  $\sim 0.30$  DU. In the afternoon of 15 May, there are a number of in situ  $\text{NO}_2$  ship spikes  $>20$  ppbv, that is, more than a fourfold increase from the morning values. A shipboard canister sample from 15 May,  $\sim 1500$  LT while passing the Petronius platform, indicated *n*-butane and *i*-pentane (species associated with flaring) that were the second highest of the campaign. However, the corresponding P66 afternoon values are confined to a 0.17–0.28 DU range, only a  $\sim 50\%$  variation and at most a factor of 2 increase from the morning. On 16 May, while passing shallow-water platforms (cf., Figure 1), the afternoon *Point Sur* shipboard spikes (label 7 in Figure 10a) are higher than on 15

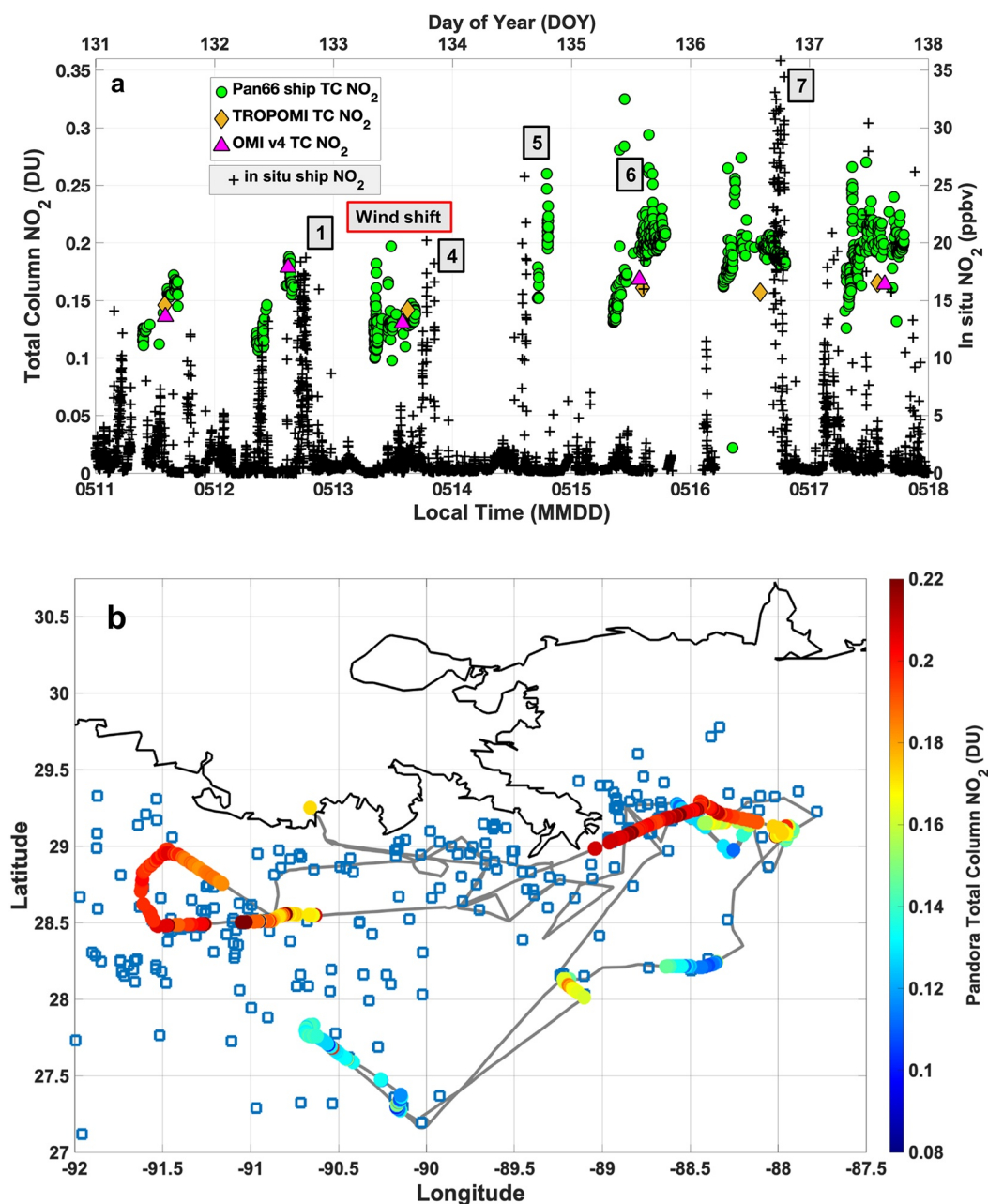


**Figure 10.** (a) Time series of TROPOMI, OMI v4, Pandora TC  $\text{NO}_2$ , and in situ  $\text{NO}_2$  during SCOAPE cruise. Pandora TC  $\text{NO}_2$  measurements and in situ data are time-matched 5-min averages. Location key same as Figures 1 and 9. (b) Pandora TC  $\text{NO}_2$  along ship track (in gray), 10–18 May 2019, during cruise. Blue squares mark locations of platforms that fall into the top 500  $\text{NO}_x$  emitters category according to the 2014 BOEM inventory (Wilson et al., 2017). The cruise segment with cleaner air (south of  $28.3^\circ\text{N}$ ; cf., Figures 4 and 5) was sampled prior to 14 May. Polluted air at and north of  $28.5^\circ\text{N}$  was sampled after 14 May.

May (near northeastern platforms, cf., Figure 1) but the corresponding P66 TC  $\text{NO}_2$  measurements do not exceed 0.20 DU.

The  $\text{NO}_2$  column densities and locations of P66 along the ship track are illustrated in Figure 10b. The location of the pre-15 May segments, mostly below 0.16 DU (green and blue dots), was in the deepwater platform area sampled with onshore winds (Figures 2 and 8a, 8d, and 8e). After 15 May, when P66 registered numerous segments with TC  $\text{NO}_2 > 0.18$  DU, sampling was closer to shore in the vicinity of platforms like Petronius and

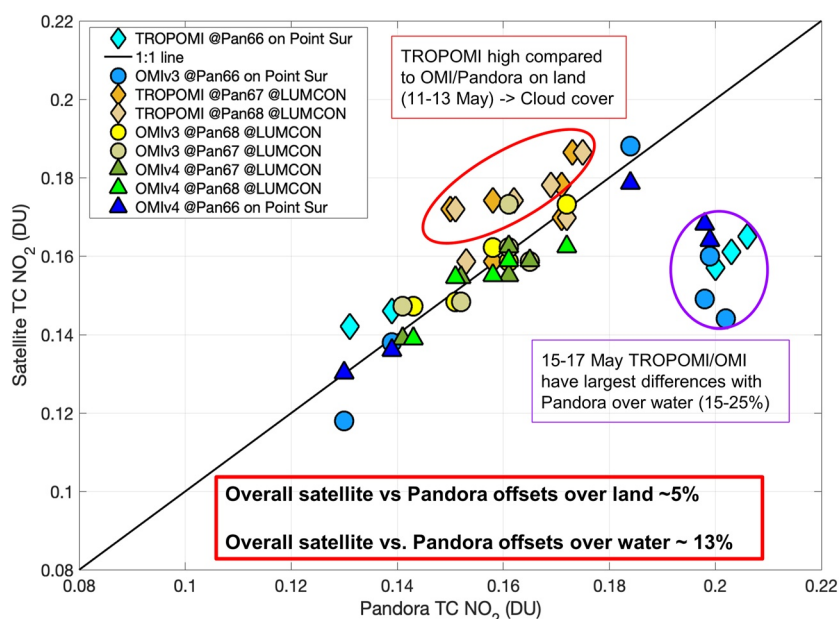


**Figure 11.** Satellites versus Pandora (Pan) 66 TC NO<sub>2</sub> on the *R/V Point Sur* during the cruise period 11–17 May 2019 with OMI v3 (light blue circles), OMI v4 (blue triangles), and TROPOMI v1.3 (cyan diamonds) readings referred to y-axis versus Pandora 66 on x-axis. Satellites versus Pandora TC NO<sub>2</sub> at LUMCON 11–17 May 2019 with: OMI v3 versus Pandora 67 (light yellow circles) and 68 (yellow circles) on the x-axis; OMI v4 versus Pandora 67 (dark green triangles) and 68 (green triangles) on the x-axis; and TROPOMI v1.3 versus Pandora 67 (gold diamonds) and 68 (tan diamonds) on the x-axis.

a high density of small natural gas operations in the northeastern and westernmost regions (orange to red in Figure 10b).

A summary of overpass comparisons from OMI and TROPOMI TC NO<sub>2</sub> relative to the shipboard Pandora 66 appears in Figure 11. Although the TROPOMI satellite instrument footprint is smaller than that of the OMI satellite, the offsets with P66 are nearly the same. During SCOAPE, a significant factor affecting Pandora-satellite agreement, summarized in Tables S1 and S2 in Supporting Information S1, was clouds. TROPOMI during 11–13 May, the cloudiest period of the cruise, recorded 20% higher TC NO<sub>2</sub> than the LUMCON P67 and P68 (tan-orange shaded diamonds in Figure 11), likely due to increased uncertainty in cloud correction in NO<sub>2</sub> retrievals. Otherwise, the satellite and Pandora TC NO<sub>2</sub> comparisons for clear-sky conditions agreed within 5%. A second factor influencing agreement was the satellite retrieval over water. As the P66 TC NO<sub>2</sub> measurements increased during 15–17 May (all symbols with Pandora TC NO<sub>2</sub> > 0.19 DU in Figure 11), the offsets were as large as 25% (satellite data low), even in cloud-free conditions. In Figure 11, the satellite data with TC NO<sub>2</sub> ≤ 0.18 DU averaged within 5% of the land and ship Pandoras.

#### 4. Summary and Conclusions

The May 2019 SCOAPE cruise, conducted with the *R/V Point Sur* in a region rich in ONG activity off the Louisiana coast, has been described. Designed to determine the feasibility of using satellite data to measure AQ with TC NO<sub>2</sub> as the key pollutant, SCOAPE addressed both scientific and technological questions.

- *What do pollutant levels measured by satellite over the GOM look like, and how do they compare to coastal Louisiana? What role does meteorology play in any observed differences?* During our May 2019 sampling, on a regional basis, the OMI and TROPOMI satellites showed that TC NO<sub>2</sub> was greater over the continent and near-coastal areas than deepwater segments of the cruise. This picture of two AQ regimes, one from 10 to 13 May and the second from 14 to 18 May, was consistent with tracers measured on the ship (ozone, CO, and VOC) and contrasting meteorology during the two periods.
- *Can satellite observations detect emissions from ONG operations, and are the measurements accurate?* The OMI and TROPOMI satellites detected elevated NO<sub>2</sub> from ONG operations on a regional basis but emissions from individual platforms could not be quantified. This limitation was due to a combination of satellite spatial

resolution, once-daily overpasses, moderately high cloud cover and low to moderate pollution levels over the GOM. Referenced to both land- and ship-based Pandoras, satellite TC NO<sub>2</sub> *on average* was accurate to ~5% and ~13%, respectively, with the satellite biased low at the higher pollution levels (differences ~20%). Under clear-sky conditions, agreement between satellites and the Pandoras was 2%–3% over the coastal site.

- *How accurately do Pandora NO<sub>2</sub> readings track short-term variations in ONG emissions? What is the precision of the new-model Pandora instruments that were deployed during SCOAPE?* Through most of a day's sampling, P66 TC NO<sub>2</sub> responds to mixed-layer NO<sub>2</sub> variability as measured with the ship's analyzer. However, timing and magnitude of the Pandora and in situ NO<sub>2</sub> responses are typically offset due to the viewing characteristics of the spectrometer. The magnitude of one set of P66 TC NO<sub>2</sub> enhancement was ~50% when corresponding NO<sub>2</sub> plumes registered a fourfold increase at the surface. In the first evaluation of Pandora TC NO<sub>2</sub> precision, three Pandora instruments, Nos. 66, 67, and 68, operating at Cocodrie, LA, for 4 weeks prior to the cruise, were found to agree within 5% (~0.01 DU) of one another.
- *Is there a difference in pollutant emissions between large, deepwater ONG platforms and the hundreds of small near-shore ONG operations?* There were strong responses in surface and Pandora NO<sub>2</sub> to both deep-water and near-shore operations. The canister sampling confirmed that near-shore platforms leak methane and other VOC associated with natural gas extraction and the deepwater platforms do not because they flare the gas.

Our analysis of the SCOAPE data has not been exhaustive, leaving room for future work. For example, the LUMCON Pandora data have not been compared to surface NO<sub>2</sub> data or the VOC samples. Evaluating the degree to which Pandora TC NO<sub>2</sub> amounts correlate with surface NO<sub>2</sub> in the GOM is a topic for further investigation. Matching the variability to sources will require analysis with in situ tracers, ancillary satellite data, air parcel trajectories, and, where possible, model output. Better statistics for the column-surface NO<sub>2</sub> connection and characterization of the environmental conditions for which the link is strongest will prepare us for optimal usage of NO<sub>2</sub> and ozone data from the upcoming geostationary Tropospheric Emissions: Monitoring of Pollution (TEMPO) satellite instrument that is designed for hourly pollution monitoring over North American coastal waters.

## Data Availability Statement

The satellite data were downloaded as follows: OMI total NO<sub>2</sub> column data from the NASA GES DISC at [https://aura.gesdisc.eosdis.nasa.gov/data/Aura\\_OMI\\_Level2/OMNO2.003](https://aura.gesdisc.eosdis.nasa.gov/data/Aura_OMI_Level2/OMNO2.003) (<https://doi.org/10.5067/Aura/OMI/DATA2017>; Krotkov et al., 2019), TROPOMI total NO<sub>2</sub> column data from <https://scihub.copernicus.eu/> (<https://doi.org/10.5270/S5P-s4ljs54>; Copernicus Sentinel-5P, 2018), and <https://worldview.earthdata.nasa.gov> provided the AIRS (AIRS Science Team/Joao Teixeira, 2013), SNPP VIIRS (Schroeder & Giglio, 2017), and MODIS products (Giglio & Justice, 2021; Naval Research Laboratory and the University of North Dakota/MODIS Adaptive Processing System [MODAPS], 2017). The SCOAPE data used here are available through the NASA/Langley Research Center Atmospheric Data Center as follows: the surface data from the LUMCON observations were retrieved from NASA/LARC/SD/ASDC (2022d; [https://doi.org/10.5067/ASDC/SUBORBITAL/SCOAPE\\_Ground\\_Data\\_1](https://doi.org/10.5067/ASDC/SUBORBITAL/SCOAPE_Ground_Data_1)), the ship data from NASA/LARC/SD/ASDC (2022a; [https://doi.org/10.5067/ASDC/SUBORBITAL/SCOAPE\\_RVPointSur\\_Data\\_1](https://doi.org/10.5067/ASDC/SUBORBITAL/SCOAPE_RVPointSur_Data_1)), and the Pandora data from NASA/LARC/SD/ASDC (2022c; [https://doi.org/10.5067/ASDC/SUBORBITAL/SCOAPE\\_Pandora\\_Data\\_1](https://doi.org/10.5067/ASDC/SUBORBITAL/SCOAPE_Pandora_Data_1)). The ozonesonde profile data are downloadable from NASA/LARC/SD/ASDC (2022b; [https://doi.org/10.5067/ASDC/SUBORBITAL/SCOAPE\\_Sondes\\_Data\\_1](https://doi.org/10.5067/ASDC/SUBORBITAL/SCOAPE_Sondes_Data_1)). HYSPLIT back trajectories (Stein et al., 2015) were run online via here: <https://www.ready.noaa.gov/hypub-bin/trajtype.pl?runtype=archive>. All analyses were performed using the MATLAB 2022b software package (<https://www.mathworks.com/help/matlab/release-notes.html>; MATLAB, 2022).

## References

- Adelman, Z. E., Pierce, R. B., Stanier, C. O., & Kenski, D. M. (2020). LMOS: 2017 Lake Michigan Ozone Study. *EM: Air and Waste Management Association's Magazine for Environmental Managers*.
- AIRS Science Team/Joao Teixeira. (2013). *AIRS/Aqua L2 standard physical retrieval (AIRS-only) V006 carbon monoxide*. NASA Worldview Earthdata. Retrieved from <https://worldview.earthdata.nasa.gov>
- Boersma, K. F., Eskes, H. J., Dirksen, R. J., van der A, R. J., Veeckind, J. P., Stammes, P., et al. (2011). An improved tropospheric NO<sub>2</sub> column retrieval algorithm for the Ozone Monitoring Instrument. *Atmospheric Measurement Techniques*, 4(9), 1905–1928. <https://doi.org/10.5194/amt-4-1905-2011>

## Acknowledgments

We are very grateful to Capt. Nic Allen, First Mate J. D. Ellington, and the entire crew of the *R/V Point Sur* and extraordinary support and hospitality from LUMCON as well as to N. Dacic (SSAI @ NASA) and V. J. Maisonet-Montañez (BOEM) for onboard measurement assistance. We thank the NASA Earth Sciences Division Tropospheric Composition Program (B. Lefer) for its support of the NASA Pandora Project as well as ESA/NASA's Pandionia Global Network and Luftblick for processing the Pandora data. This study was partially funded by the US Department of the Interior, Bureau of Ocean Energy Management through Interagency Agreement with NASA/Goddard: M17PG0026 (B. N. Duncan, PI); M123PG0001 (R. M. Stauffer, PI). Additional support came from the NASA HQ Applied Sciences Program (J. Haynes).



- Boersma, K. F., Eskes, H. J., Richter, A., De Smedt, I., Lorente, A., Beirle, S., et al. (2018). Improving algorithms and uncertainty estimates for satellite NO<sub>2</sub> retrievals: Results from the quality assurance for the essential climate variables (QA4ECV) project. *Atmospheric Measurement Techniques*, 11(12), 6651–6678. <https://doi.org/10.5194/amt-11-6651-2018>
- Boersma, K. F., Eskes, H. J., Veefkind, J. P., Brinksma, E. J., van der A, R. J., Sneep, M., et al. (2007). Near-real time retrieval of tropospheric NO<sub>2</sub> from OMI. *Atmospheric Chemistry and Physics*, 7(8), 2103–2118. <https://doi.org/10.5194/acp-7-2103-2007>
- Burrows, J. P., Weber, M., Buchwitz, M., Rozanov, V., Ladstaetter-Weissenmayer, A., Richter, A., et al. (1999). The global ozone monitoring experiment (GOME): Mission concept and first scientific results. *Journal of the Atmospheric Sciences*, 56(2), 151–175. [https://doi.org/10.1175/1520-0469\(1999\)056<0151:TGOMEG>2.0.CO;2](https://doi.org/10.1175/1520-0469(1999)056<0151:TGOMEG>2.0.CO;2)
- Choi, S., Lamsal, L. N., Follette-Cook, M., Joiner, J., Krotkov, N. A., Swartz, W. H., et al. (2020). Assessment of NO<sub>2</sub> observations during DISCOVER-AQ and KORUS-AQ field campaigns. *Atmospheric Measurement Techniques*, 13(5), 2523–2546. <https://doi.org/10.5194/amt-13-2523-2020>
- Colman, J. J., Swanson, A. L., Meinardi, S., Sive, B. C., Blake, D. R., & Rowland, F. S. (2001). Description of the analysis of a wide range of volatile organic compounds in whole air samples collected during PEM-tropics A and B. *Analytical Chemistry*, 73(N15), 3723–3731. <https://doi.org/10.1021/ac010027g>
- Copernicus Sentinel-5P (processed by ESA). (2018). *TROPOMI level 2 nitrogen dioxide total column products, version 01.3*. European Space Agency. <https://doi.org/10.5270/S5P-s4ljg54>
- Dacic, S., Sullivan, J. T., Knowland, K. E., Wolfe, G. M., Oman, L. D., Berkoff, T. A., & Gronoff, G. P. (2020). Evaluation of NASA's high-resolution global composition simulations: Understanding a pollution event in the Chesapeake Bay during the summer 2017 OWLETS campaign. *Atmospheric Environment*, 222, 117133. <https://doi.org/10.1016/j.atmosenv.2019.117133>
- Duncan, B. N. (2020). NASA resources to monitor offshore and coastal air quality. In *OCS Study BOEM 2020-046* (p. 41). U.S. Department of the Interior, Bureau of Ocean Energy Management.
- Duncan, B. N., Lamsal, L. N., Thompson, A. M., Yoshida, Y., Lu, Z., Streets, D. G., et al. (2016). A space-based, high-resolution view of notable changes in urban NO<sub>2</sub> pollution around the world (2005–2014). *Journal of Geophysical Research: Atmospheres*, 121, 976–996. <https://doi.org/10.1002/2015JD024121>
- Duncan, B. N., Yoshida, Y., De Foy, B., Lamsal, L. N., Streets, D. G., Lu, Z., et al. (2013). The observed response of ozone monitoring instrument (OMI) NO<sub>2</sub> columns to NO<sub>x</sub> emission controls on power plants in the United States: 2005–2011. *Atmospheric Environment*, 81, 102–111. <https://doi.org/10.1016/j.atmosenv.2013.08.068>
- Flynn, C. M., Pickering, K. E., Crawford, J. H., Lamsal, L., Krotkov, N., Herman, J., et al. (2014). Relationship between column-density and surface mixing ratio: Statistical analysis of O<sub>3</sub> and NO<sub>2</sub> data from the July 2011 DISCOVER-AQ mission. *Atmospheric Environment*, 92, 429–441. <https://doi.org/10.1016/j.atmosenv.2014.04.041>
- Giglio, L., & Justice, C. (2021). MODIS/Aqua Thermal Anomalies/Fire 5-Min L2 Swath 1km V061 [Dataset]. NASA Worldview Earthdata. Retrieved from <https://worldview.earthdata.nasa.gov>
- Goldberg, D. L., Anenberg, S. C., Griffin, D., McLinden, C. A., Lu, Z., & Streets, D. G. (2020). Disentangling the impact of the COVID-19 lockdowns on urban NO<sub>2</sub> from natural variability. *Geophysical Research Letters*, 47, e2020GL089269. <https://doi.org/10.1029/2020GL089269>
- Goldberg, D. L., Anenberg, S. C., Kerr, G. H., Moheggh, A., Lu, Z., & Streets, D. G. (2021). TROPOMI NO<sub>2</sub> in the United States: A detailed look at the annual averages, weekly cycles, effects of temperature, and correlation with surface NO<sub>2</sub> concentrations. *Earth's Future*, 9, e2020EF001665. <https://doi.org/10.1029/2020EF001665>
- Gronoff, G., Robinson, J., Berkoff, T., Swap, R., Farris, B., Schroeder, J., et al. (2019). A method for quantifying near range point source induced O<sub>3</sub> titration events using co-located Lidar and Pandora measurements. *Atmospheric Environment*, 204, 43–52. <https://doi.org/10.1016/j.atmosenv.2019.01.052>
- Herman, J., Abuhassan, N., Kim, J., Kim, J., Dubey, M., Raponi, M., & Tzortziou, M. (2019). Underestimation of column NO<sub>2</sub> amounts from the OMI satellite compared to diurnally varying ground-based retrievals from multiple PANDORA spectrometer instruments. *Atmospheric Measurement Techniques*, 12(10), 5593–5612. <https://doi.org/10.5194/amt-12-5593-2019>
- Herman, J., Cede, A., Spinei, E., Mount, G., Tzortziou, M., & Abuhassan, N. (2009). NO<sub>2</sub> column amounts from ground-based Pandora and MFDOAS spectrometers using the direct-sun DOAS technique: Intercomparisons and application to OMI validation. *Journal of Geophysical Research*, 114, D13307. <https://doi.org/10.1029/2009JD011848>
- Herman, J., Spinei, E., Fried, A., Kim, J., Kim, J., Kim, W., et al. (2018). NO<sub>2</sub> and HCHO measurements in Korea from 2012 to 2016 from PSI spectrometer instruments compared with OMI retrievals and with aircraft measurements during the KORUS-AQ campaign. *Atmospheric Measurement Techniques*, 1–60. <https://doi.org/10.5194/amt-2018-56>
- Heue, K.-P., Wagner, T., Broccardo, S. P., Walter, D., Pketh, S. J., Ross, K. E., et al. (2008). Direct observation of two dimensional trace gas distributions with an airborne imaging DOAS instrument. *Atmospheric Chemistry and Physics*, 8(22), 6707–6717. <https://doi.org/10.5194/acp-8-6707-2008>
- Judd, L. M., Al-Saadi, J. A., Janz, S. J., Kowalewski, M. G., Pierce, R. B., Szykman, J. J., et al. (2019). Evaluating the impact of spatial resolution on tropospheric NO<sub>2</sub> column comparisons within urban areas using high-resolution airborne data. *Atmospheric Measurement Technology*, 12(11), 6091–6111. <https://doi.org/10.5194/amt-12-6091-2019>
- Judd, L. M., Al-Saadi, J. A., Szykman, J. J., Valin, L. C., Janz, S. J., Kowalewski, M. G., et al. (2020). Evaluating Sentinel-5P TROPOMI tropospheric NO<sub>2</sub> column densities with airborne and Pandora spectrometers near New York City and Long Island Sound. *Atmospheric Measurement Techniques*, 13(11), 6113–6140. <https://doi.org/10.5194/amt-2020-151>
- Karambelas, A. (2020). LISTOS: Toward a better understanding of New York City's ozone pollution problem. *EM Magazine (Air and Waste Management Assn)*. Retrieved from [https://airandwmapa.sharepoint.com/:b/s/AWMA\\_Website/EfnNGMYV4itAp6XX5QFGKq8B6bOiuLv8wUNdQAXjaRb0eg?e=OgNqAK](https://airandwmapa.sharepoint.com/:b/s/AWMA_Website/EfnNGMYV4itAp6XX5QFGKq8B6bOiuLv8wUNdQAXjaRb0eg?e=OgNqAK)
- Kebabian, P. L., Herndon, S. C., & Freedman, A. (2005). Detection of nitrogen dioxide by cavity attenuated phase shift spectroscopy. *Analytical Chemistry*, 77(2), 724–728. <https://doi.org/10.1021/ac048715y>
- Knepp, T., Pippin, M., Crawford, J., Chen, G., Szykman, J., Long, R., et al. (2015). Estimating surface NO<sub>2</sub> and SO<sub>2</sub> mixing ratios from fast-response total column observations and potential application to geostationary missions. *Journal of Atmospheric Chemistry*, 72(3–4), 261–286. <https://doi.org/10.1007/s10874-013-9257-6>
- Kollonige, D. E., Thompson, A. M., Josipovic, M., Tzortziou, M., Beukes, J. P., Burger, R., et al. (2018). OMI satellite and ground-based Pandora observations and their application to surface NO<sub>2</sub> estimations at terrestrial and marine sites. *Journal of Geophysical Research: Atmospheres*, 123, 1441–1459. <https://doi.org/10.1002/2017JD026518>
- Kotsakis, A., Sullivan, J. T., Hanisco, T. F., Swap, R. J., Caicedo, V., Berkoff, T. A., et al. (2022). Sensitivity of total column NO<sub>2</sub> at a marine site within the Chesapeake Bay during OWLETS-2. *Atmospheric Environment*, 277, 119063. <https://doi.org/10.1016/j.atmosenv.2022.119063>

- Kreher, K., Spinei, E., Piters, A., Apituley, A., Bais, A., Doerner, S., et al. (2020). MAX-DOAS measurements of atmospheric rural and urban NO<sub>2</sub> gradients during the TROLIX'19 campaign. *Paper presented at EGU General Assembly 2020*, (p. EGU2020-20796). <https://doi.org/10.5194/egusphere-egu2020-20796>
- Krotkov, N. A., Lamsal, L. N., Celarier, E. A., Swartz, W. H., Marchenko, S. V., Bucsela, E. J., et al. (2017). The version 3 OMI NO<sub>2</sub> standard product. *Atmospheric Measurement Technology*, 10(9), 3133–3149. <https://doi.org/10.5194/amt-10-3133-2017>
- Krotkov, N. A., Lamsal, L. N., Marchenko, S. V., Bucsela, E. J., Swartz, W. H., & Joiner, J., & The OMI Core Team. (2019). *OMI/Aura nitrogen dioxide (NO<sub>2</sub>) total and tropospheric column 1-orbit L2 swath 13x24 km V003*. Goddard Earth Sciences Data and Information Services Center (GES DISC). <https://doi.org/10.5067/Aura/OMI/DATA2017>
- Lamsal, L. N., Janz, S., Krotkov, N., Pickering, K. E., Spurr, R. J. D., Kowalewski, M., et al. (2017). High-resolution NO<sub>2</sub> observations from the airborne compact atmospheric mapper: Retrieval and validation. *Journal of Geophysical Research: Atmospheres*, 122, 1953–1970. <https://doi.org/10.1002/2016JD025483>
- Lamsal, L. N., Krotkov, N. A., Celarier, E. A., Swartz, W. H., Pickering, K. E., Bucsela, E. J., et al. (2014). Evaluation of OMI operational standard NO<sub>2</sub> column retrievals using in situ and surface-based NO<sub>2</sub> observations. *Atmospheric Chemistry and Physics*, 14(21), 11587–11609. <https://doi.org/10.5194/acp-14-11587-2014>
- Lamsal, L. N., Krotkov, N. A., Vasilkov, A., Marchenko, S., Qin, W., Yang, E.-S., et al. (2021). Ozone Monitoring Instrument (OMI) Aura nitrogen dioxide standard product version 4.0 with improved surface and cloud treatments. *Atmospheric Measurement Techniques*, 14(1), 455–479. <https://doi.org/10.5194/amt-14-455-2021>
- Levelt, P. F., Joiner, J., Tamminen, J., Veefkind, J. P., Bhartia, P. K., Zweers, D. C. S., et al. (2018). The ozone monitoring instrument: Overview of 14 years in space. *Atmospheric Chemistry and Physics*, 18(8), 5699–5745. <https://doi.org/10.5194/acp-18-5699-2018>
- Levelt, P. F., Van den Oord, G. H. J., Dobber, M. R., Malkki, A., Visser, H., De Vries, J., et al. (2006). The ozone monitoring instrument. *IEEE Transactions on Geoscience and Remote Sensing*, 44(5), 1093–1101. <https://doi.org/10.1109/tgrs.2006.872333>
- Luftblick. (2019a). Fiducial reference measurements for air quality. Retrieved from [https://www.pandonia-global-network.org/wp-content/uploads/2021/01/LuftBlick\\_FRM4AQ\\_InstrumentChangeUpgrade\\_RP\\_2019002\\_v4.pdf](https://www.pandonia-global-network.org/wp-content/uploads/2021/01/LuftBlick_FRM4AQ_InstrumentChangeUpgrade_RP_2019002_v4.pdf)
- Luftblick. (2019b). Fiducial reference measurements for air quality TN on data quality flagging generic procedure evolution. Retrieved from [https://www.pandonia-global-network.org/wp-content/uploads/2022/02/LuftBlick\\_FRM4AQ\\_DataQualityFlaggingGenericProcedureEvolution\\_TN\\_2019008\\_v5.pdf](https://www.pandonia-global-network.org/wp-content/uploads/2022/02/LuftBlick_FRM4AQ_DataQualityFlaggingGenericProcedureEvolution_TN_2019008_v5.pdf)
- Luftblick. (2021). Pandonia Global Network data products Readme document version 1.8-3. Retrieved from [https://www.pandonia-global-network.org/wp-content/uploads/2021/01/PGN\\_DataProducts\\_Readme\\_v1-8-3.pdf](https://www.pandonia-global-network.org/wp-content/uploads/2021/01/PGN_DataProducts_Readme_v1-8-3.pdf)
- Luftblick. (2022). Fiducial reference measurements for air quality. Retrieved from [https://www.pandonia-global-network.org/wp-content/uploads/2022/08/LuftBlick\\_FRM4AQ\\_NewAlgorithmPlan-ATBD\\_RP\\_2019005\\_v7.pdf](https://www.pandonia-global-network.org/wp-content/uploads/2022/08/LuftBlick_FRM4AQ_NewAlgorithmPlan-ATBD_RP_2019005_v7.pdf)
- Martins, D. K., Najjar, R. G., Tzortziou, M., Abuhassan, N., Thompson, A. M., & Kollonige, D. E. (2016). Spatial and temporal variability of ground and satellite column measurements of NO<sub>2</sub> and O<sub>3</sub> over the Atlantic Ocean during the Deposition of Atmospheric Nitrogen to Coastal Ecosystems Experiment (DANCE). *Journal of Geophysical Research: Atmospheres*, 121, 14175–14187. <https://doi.org/10.1002/2016JD024998>
- Martins, D. K., Stauffer, R. M., Thompson, A. M., Knepp, T. N., & Pippin, M. (2012). Surface ozone at a coastal suburban site in 2009 and 2010: Relationships to chemical and meteorological processes. *Journal of Geophysical Research*, 117, D05306. <https://doi.org/10.1029/2011JD016828>
- MATLAB. (2022). MATLAB version 9.13.0.2126072 (R2022b) [Software]. The Mathworks, Inc. Retrieved from <https://www.mathworks.com/help/matlab/release-notes.html>
- NASA/LARC/SD/ASDC. (2022a). SCOAPE Balloon and Ozone sondes Data [Dataset]. NASA Langley Atmospheric Science Data Center DAAC. [https://doi.org/10.5067/ASDC/SUBORBITAL/SCOAPE\\_Sondes\\_Data\\_1](https://doi.org/10.5067/ASDC/SUBORBITAL/SCOAPE_Sondes_Data_1)
- NASA/LARC/SD/ASDC. (2022b). SCOAPE Ground Site Data [Dataset]. NASA Langley Atmospheric Science Data Center DAAC. [https://doi.org/10.5067/ASDC/SUBORBITAL/SCOAPE\\_Ground\\_Data\\_1](https://doi.org/10.5067/ASDC/SUBORBITAL/SCOAPE_Ground_Data_1)
- NASA/LARC/SD/ASDC. (2022c). SCOAPE Pandora Column Observations [Dataset]. NASA Langley Atmospheric Science Data Center DAAC. [https://doi.org/10.5067/ASDC/SUBORBITAL/SCOAPE\\_Pandora\\_Data\\_1](https://doi.org/10.5067/ASDC/SUBORBITAL/SCOAPE_Pandora_Data_1)
- NASA/LARC/SD/ASDC. (2022d). SCOAPE R/V Point Sur Data [Dataset]. NASA Langley Atmospheric Science Data Center DAAC. [https://doi.org/10.5067/ASDC/SUBORBITAL/SCOAPE\\_RVPointSur\\_Data\\_1](https://doi.org/10.5067/ASDC/SUBORBITAL/SCOAPE_RVPointSur_Data_1)
- Naval Research Laboratory and the University of North Dakota/MODIS Adaptive Processing System (MODAPS). (2017). MODIS/Terra Aqua value-added Aerosol Optical Depth (MCD40DHD) [Dataset]. NASA Worldview Earthdata. <https://doi.org/10.5067/MODIS/MCD40DHD.NRT.061>
- Nowlan, C. R., Liu, X., Leitch, J. W., Chance, K., Gonzalez, A. G., Liu, C., et al. (2016). Nitrogen dioxide observations from the Geostationary Trace gas and Aerosol Sensor Optimization (GeoTASO) airborne instrument: Retrieval algorithm and measurements during DISCOVER-AQ Texas 2013. *Atmospheric Measurement Techniques*, 9(6), 2647–2668. <https://doi.org/10.5194/amt-9-2647-2016>
- Petropavlovskikh, I., Ray, E., Davis, S. M., Rosenlof, K., Manney, G., Shetter, R., et al. (2010). Low ozone bubbles observed in the tropical tropopause layer during the TC4 campaign in 2007. *Journal of Geophysical Research*, 115, D00J16. <https://doi.org/10.1029/2009JD012804>
- Piters, A. J. M., Boersma, K. F., Kroon, M., Hains, J. C., Van Roozendael, M., Wittrock, F., et al. (2012). The Cabauw Intercomparison campaign for Nitrogen Dioxide measuring Instruments (CINDI): Design, execution, and early results. *Atmospheric Measurement Technology*, 5(2), 457–485. <https://doi.org/10.5194/amt-5-457-2012>
- Platt, U., & Stutz, J. (2008). *Differential optical absorption spectroscopy principles and applications*. Springer-Verlag. Retrieved from <http://www.springer.com/environmental+engineering+and+physics/book/978-3-540-21193-8>
- Reed, A. J., Thompson, A. M., Kollonige, D. E., Martins, D. K., Tzortziou, M. A., Herman, J. R., et al. (2015). Effects of local meteorology and aerosols on ozone and nitrogen dioxide retrievals from OMI and Pandora spectrometers in Maryland, USA during DISCOVER-AQ 2011. *Journal of Atmospheric Chemistry*, 72(3–4), 455–482. <https://doi.org/10.1007/s10874-013-9254-9>
- Robinson, J., Kotsakis, A., Santos, F., Swap, R. J., Knowland, K. E., Labow, G., et al. (2020). Using networked Pandora observations to capture spatiotemporal changes in total column ozone associated with stratosphere-to-troposphere transport. *Atmospheric Research*, 238, 104872. <https://doi.org/10.1016/j.atmosres.2020.104872>
- Russell, A. R., Valin, L. C., & Cohen, R. C. (2012). Trends in OMI NO<sub>2</sub> observations over the United States: Effects of emission control technology and the economic recession. *Atmospheric Chemistry and Physics*, 12(24), 12197–12209. <https://doi.org/10.5194/acp-12-12197-2012>
- Schroeder, W., & Giglio, L. (2017). VIIRS/NPP Thermal Anomalies/Fire 6-Min L2 Swath 750m V001 [Dataset]. NASA Worldview Earthdata. Retrieved from <https://worldview.earthdata.nasa.gov>
- Spinei, E., Tiefengraber, M., Müller, M., Gebetsberger, M., Cede, A., Valin, L., et al. (2021). Effect of polyoxymethylene (POM-H Delrin) off-gassing within the Pandora head sensor on direct-sun and multi-axis formaldehyde column measurements in 2016–2019. *Atmospheric Measurement Techniques*, 14(1), 647–663. <https://doi.org/10.5194/amt-14-647-2021>

- Stanier, C. O., Pierce, R. B., Abdi-Oskouei, M., Adelman, Z. E., Al-Saadi, J., Alwe, H. D., et al. (2021). Overview of the lake Michigan ozone study 2017. *Bulletin of the American Meteorological Society*, 102(12), E2207–E2225. <https://doi.org/10.1175/BAMS-D-20-0061.1>
- Stein, A. F., Draxler, R. R., Rolph, G. D., Stunder, B. J. B., Cohen, M. D., & Ngan, F. (2015). NOAA's HYSPLIT atmospheric transport and dispersion modeling system. *Bulletin of the American Meteorological Society*, 96(12), 2059–2077. <https://doi.org/10.1175/BAMS-D-14-00110.1>
- Sullivan, J. T., Berkoff, T., Gronoff, G., Knepp, T., Pippin, M., Allen, D., et al. (2018). The Ozone Water-Land Environmental Transition Study (OWLETS): An innovative strategy for understanding Chesapeake Bay pollution events. *Bulletin of the American Meteorological Society*, 100(2), 291–306. <https://doi.org/10.1175/BAMS-D-18-0025>
- Sullivan, J. T., Dreessen, J., Berkoff, T., Delgado, R., Ren, X., & Aburn, G., Jr. (2020). OWLETS-2: An enhanced monitoring strategy directly within the Chesapeake Bay. *EM Magazine (Air and Waste Management Assn)*. Retrieved from [https://airandwmapa.sharepoint.com/b:/s/AWMA\\_Website/EcM\\_RQKzLoBMjMZpvYQ58QcBrHxc7gaWOHwPflcKDFrMBQ?e=MbVyuH](https://airandwmapa.sharepoint.com/b:/s/AWMA_Website/EcM_RQKzLoBMjMZpvYQ58QcBrHxc7gaWOHwPflcKDFrMBQ?e=MbVyuH)
- Tack, F., Merlaud, A., Meier, A. C., Vlemmix, T., Ruhtz, T., Iordache, M.-D., et al. (2019). Intercomparison of four airborne imaging DOAS systems for tropospheric NO<sub>2</sub> mapping—The AROMAPEX campaign. *Atmospheric Measurement Techniques*, 12(1), 211–236. <https://doi.org/10.5194/amt-12-211-2019>
- Thompson, A. M. (2020). Evaluation of NASA's remote-sensing capabilities in coastal environments. *OCS Study BOEM 2020-047* (p. 49). Retrieved from [https://espis.boem.gov/final%20reports/BOEM\\_2020-047.pdf](https://espis.boem.gov/final%20reports/BOEM_2020-047.pdf)
- Thompson, A. M., Doddridge, B. G., Witte, J. C., Hudson, R. D., Luke, W. T., Johnson, J. E., et al. (2000). A tropical Atlantic paradox: Ship-board and satellite views of a tropospheric ozone maximum and wave-one in January–February 1999. *Geophysical Research Letters*, 27(20), 3317–3320. <https://doi.org/10.1029/1999GL011273>
- Thompson, A. M., Kollonige, D. E., Stauffer, R. M., Abuhassan, N., Kotsakis, A. E., Swap, R. J., & Wecht, H. E. (2020). Satellite and ship-board views of air quality along the Louisiana coast: The 2019 SCOAPE (Satellite Coastal and Oceanic Atmospheric Pollution Experiment) cruise. *EM Magazine (Air and Waste Management Assn)*. Retrieved from [https://airandwmapa.sharepoint.com/b:/s/AWMA\\_Website/EXUfo17X0Y5NunTME6afwDQBAYhAQGLIX9XaxXXsbAxo9dA?e=IcAmhG](https://airandwmapa.sharepoint.com/b:/s/AWMA_Website/EXUfo17X0Y5NunTME6afwDQBAYhAQGLIX9XaxXXsbAxo9dA?e=IcAmhG)
- Thompson, A. M., MacFarlane, A. M., Morris, G. A., Yorks, J. E., Miller, S. K., Taubman, B. F., et al. (2010). Convective and wave signatures in ozone profiles over the equatorial Americas: Views from TC4 (2007) and SHADOZ. *Journal of Geophysical Research*, 115, D00J23. <https://doi.org/10.1029/2009JD012909>
- Thompson, A. M., Miller, S. K., Tilmes, S., Kollonige, D. W., Witte, J. C., Oltmans, S. J., et al. (2012). Southern Hemisphere Additional Ozone sondes (SHADOZ) ozone climatology (2005–2009): Tropospheric and tropical tropopause layer (TTL) profiles with comparisons to OMI-based ozone products. *Journal of Geophysical Research*, 117, D23301. <https://doi.org/10.1029/2010JD016911>
- Thompson, A. M., Smit, H. G. J., Witte, J. C., Stauffer, R. M., Johnson, B. J., Morris, G. A., et al. (2019). Ozone sonde quality assurance: The JOSIE-SHADOZ (2017) experience. *Bulletin of the American Meteorological Society*, 100(1), 155–171. <https://doi.org/10.1175/BAMS-17-0311>
- Thompson, A. M., Stauffer, R. M., Boyle, T. P., Kollonige, D. E., Miyazaki, K., Tzortziou, M. A., et al. (2019). Comparison of near-surface NO<sub>2</sub> pollution with Pandora total column NO<sub>2</sub> during the Korea–United States Ocean Color (KORUS OC) campaign. *Journal of Geophysical Research: Atmospheres*, 124, 13560–13575. <https://doi.org/10.1029/2019JD030765>
- Tirpitz, J.-L., Frieß, U., Hendrick, F., Alberti, C., Allaart, M., Apituley, A., et al. (2021). Intercomparison of MAX-DOAS vertical profile retrieval algorithms: Studies on field data from the CINDI-2 campaign. *Atmospheric Measurement Techniques*, 14, 1–35. <https://doi.org/10.5194/amt-14-1-2021>
- Tong, D. Q., Lamsal, L., Pan, L., Ding, C., Kim, H., Lee, P., et al. (2015). Long-term NO<sub>x</sub> trends over large cities in the United States during the great recession: Comparison of satellite retrievals, ground observations, and emission inventories. *Atmospheric Environment*, 107, 70–84. <https://doi.org/10.1016/j.atmosenv.2015.01.035>
- Tzortziou, M., Herman, J. R., Loughner, C. P., Cede, A., Abuhassan, N., & Naik, S. (2015). Spatial and temporal variability of ozone and nitrogen dioxide over a major urban estuarine ecosystem. *Journal of Atmospheric Chemistry*, 72(3–4), 287–309. <https://doi.org/10.1007/s10874-013-9255-8>
- Tzortziou, M., Parker, O., Lamb, B., Herman, J., Lamsal, L., Stauffer, R., & Abuhassan, N. (2018). Atmospheric trace gas (NO<sub>2</sub> and O<sub>3</sub>) variability in Korean coastal waters, implications for remote sensing of coastal ocean color dynamics. *Remote Sensing*, 10, 1587. <https://doi.org/10.3390/rs10101587>
- Tzortziou, M., Thompson, A. M., & Herman, J. (2015). Dynamics of atmospheric trace gases and aerosols in Korean coastal waters: Impacts on ocean color atmospheric correction and surface air pollution studies (NASA Project Description, Grant # NNX16AD60G, PI: Tzortziou).
- van Geffen, J., Eskes, H., Compennolle, S., Pinardi, G., Verhoelst, T., Lambert, J. C., et al. (2022). Sentinel-5P TROPOMI NO<sub>2</sub> retrieval: Impact of version v2.2 improvements and comparisons with OMI and ground-based data. *Atmospheric Measurement Techniques*, 15(7), 2037–2060. <https://doi.org/10.5194/amt-15-2037-2022>
- van Geffen, J., Eskes, H. J., Boersma, K. F., Maasakkers, J. D., & Veefkind, J. P. (2018). *TROPOMI ATBD of the total and tropospheric NO<sub>2</sub> data products (issue 1.2.0)*. Royal Netherlands Meteorological Institute (KNMI). Retrieved from [http://www.tropomi.eu/sites/default/files/files/publicS5P-KNMI-L2-0005-RP-ATBD\\_NO2\\_data\\_products-20190206\\_v140.pdf](http://www.tropomi.eu/sites/default/files/files/publicS5P-KNMI-L2-0005-RP-ATBD_NO2_data_products-20190206_v140.pdf)
- Veefkind, J., Aben, I., McMullan, K., Forster, H., de Vries, J., Otter, G., et al. (2012). TROPOMI on the ESA Sentinel-5 precursor: A GMES mission for global observations of the atmospheric composition for climate, air quality and ozone layer applications. *Remote Sensing of Environment*, 120, 70–83. <https://doi.org/10.1016/j.rse.2011.09.027>
- Verhoelst, T., Compennolle, S., Pinardi, G., Lambert, J.-C., Eskes, H. J., Eichmann, K.-U., et al. (2021). Ground-based validation of the Copernicus Sentinel-5P TROPOMI NO<sub>2</sub> measurements with the NDACC ZSL-DOAS, MAX-DOAS and Pandora Global Networks. *Atmospheric Measurement Techniques*, 14(1), 481–510. <https://doi.org/10.5194/amt-14-481-2021>
- Wilson, D., Billings, R., Chang, R., Do, B., Enoch, S., Perez, H., & Sellers, J. (2019). *Year 2017 emissions inventory study*. OCS Study BOEM 2019-072 (231 pp.). US Department of the Interior, Bureau of Ocean Energy Management. Retrieved from [https://espis.boem.gov/final%20reports/BOEM\\_2019-072.pdf](https://espis.boem.gov/final%20reports/BOEM_2019-072.pdf)
- Wilson, D., Billings, R., Chang, S., Enoch, B., Do, H., Perez, H., & Sellers, J. (2017). *Year 2014 Gulfwide emissions inventory study*. OCS Study BOEM 2017-044 (p. 275). US Department of the Interior, Bureau of Ocean Energy Management, Gulf of Mexico OCS Region. Retrieved from <https://www.boem.gov/environment/environmental-studies/2014-gulfwide-emission-inventory>
- Yacovitch, T., Daube, C., & Herndon, S. (2020). Methane emissions from offshore oil and gas platforms in the Gulf of Mexico. *Environmental Science & Technology*, 54(6), 3530–3538. <https://doi.org/10.1021/acs.est.9b07148>
- Yarnes, C. (2013).  $\delta^{13}\text{C}$  and  $\delta^2\text{H}$  measurement of methane from ecological and geological sources by gas chromatography/combustion/pyrolysis isotope-ratio mass spectrometry. *Rapid Communications in Mass Spectrometry*, 27(9), 1036–1044. <https://doi.org/10.1002/rcm.6549>